



HAL
open science

Maize ATR safeguards genome stability during kernel development to prevent early endosperm endocycle onset and cell death

Jose Antonio Pedroza-Garcia, Thomas Eekhout, Ignacio Achon, Maher-Un Nisa, Griet Coussens, Hilde van den Daele, Laurens Pauwels, Mieke van Lijsebettens, Cécile Raynaud, Lieven de Veylder

► To cite this version:

Jose Antonio Pedroza-Garcia, Thomas Eekhout, Ignacio Achon, Maher-Un Nisa, Griet Coussens, et al.. Maize ATR safeguards genome stability during kernel development to prevent early endosperm endocycle onset and cell death. *The Plant cell*, 2021, 33 (8), pp.1-63. 10.1093/plcell/koab158 . hal-03323715

HAL Id: hal-03323715

<https://hal.science/hal-03323715>

Submitted on 22 Aug 2021

HAL is a multi-disciplinary open access archive for the deposit and dissemination of scientific research documents, whether they are published or not. The documents may come from teaching and research institutions in France or abroad, or from public or private research centers.

L'archive ouverte pluridisciplinaire **HAL**, est destinée au dépôt et à la diffusion de documents scientifiques de niveau recherche, publiés ou non, émanant des établissements d'enseignement et de recherche français ou étrangers, des laboratoires publics ou privés.



Distributed under a Creative Commons Attribution 4.0 International License

1 **Maize ATR Safeguards Genome Stability During Kernel Development to Prevent Early**
2 **Endosperm Endocycle Onset and Cell Death^[W]**

3

4 **AUTHORS:**

5 Jose Antonio Pedroza-Garcia,^{a,b} Thomas Eekhout,^{a,b} Ignacio Achon,^{a,b} Maher-Un Nisa,^c Griet
6 Coussens,^{a,b} Hilde Van den Daele,^{a,b} Laurens Pauwels,^{a,b} Mieke Van Lijsebettens,^{a,b} Cécile
7 Raynaud,^c and Lieven De Veylder^{a,b,1}

8 **AFFILIATIONS:**

9 ^aDepartment of Plant Biotechnology and Bioinformatics, Ghent University, Ghent, B-9052,
10 Belgium

11 ^bCenter for Plant Systems Biology, VIB, Ghent, B-9052, Belgium

12 ^cInstitute of Plant Sciences Paris-Saclay (IPS2), CNRS, INRA, University Paris-Sud, University of
13 Evry, Paris University, Sorbonne Paris-Cite, University of Paris-Saclay, Batiment 630, 91405,
14 Orsay, France

15 **ORCID IDs:** 0000-0001-8258-0157 (J.A.P.G.); 0000-0002-2878-1553 (T.E.); 0000-0002-4553-
16 1257 (I.A.); 0000-0002-6135-4836 (M.-U.N.); 0000-0003-2285-5782 (G.C.); 0000-0002-4271-
17 6694 (H.V.D.); 0000-0002-0221-9052 (L.P.); 0000-0002-7632-1463 (M.V.L.); 0000-0002-5231-
18 8120 (C.R.); 0000-0003-1150-4426 (L.D.V.)

19 **RUNNING TITLE:** Maize ATR controls endosperm development

20 **ONE-SENTENCE SUMMARY:** Differently from Arabidopsis, maize ATR activity plays an
21 essential role under control growth conditions, ensuring genome stability during kernel
22 development.

23

24 **CORRESPONDING AUTHOR:**

25 Lieven De Veylder

26 Center for Plant Systems Biology

27 VIB-Ghent University

28 Technologiepark 71, B-9052 Gent (Belgium).

29 Tel.: +32 9 3313800; Fax: +32 9 3313809; E-mail: lieven.deveyllder@psb.vib-ugent.be

30

31 **FOOTNOTES:**

32 ¹Address correspondence to lieven.deveyllder@psb.vib-ugent.be

33 The author responsible for distribution of materials integral to the findings presented in this article in
34 accordance with the policy described in the Instructions for Authors (www.plantcell.org) is: Lieven
35 De Veylder (lieven.deveyllder@psb.vib-ugent.be).

36 [W]Online version contains Web-only data.

37 **ABSTRACT**

38

39 **The Ataxia-telangiectasia mutated (ATM) and ATM and Rad3-related (ATR) kinases**
40 **coordinate the DNA damage response (DDR). The roles described for *Arabidopsis thaliana***
41 **ATR and ATM are assumed to be conserved over other plant species, but molecular evidence**
42 **is scarce. Here, we demonstrate that the functions of ATR and ATM are only partially**
43 **conserved between Arabidopsis and maize. In both species, ATR and ATM play a key role in**
44 **DNA repair and cell cycle checkpoint activation, but whereas Arabidopsis plants do not suffer**
45 **from the absence of ATR under control growth conditions, maize mutant plants accumulate**
46 **replication defects, likely due to their large genome size. Moreover, contrarily to Arabidopsis,**
47 **maize ATM deficiency does not trigger meiotic defects, whereas the ATR kinase appears to be**
48 **crucial for the maternal fertility. Strikingly, ATR is required to repress premature endocycle**
49 **onset and cell death in the maize endosperm. Its absence results in a reduction of kernel size,**
50 **protein and starch content, and a stochastic lethality of kernels, a process being counteracted**
51 **by ATM. Additionally, whereas Arabidopsis *atr atm* double mutants are viable, no such**
52 **mutants could be obtained for maize. Therefore, our data highlight that the mechanisms**
53 **maintaining genome integrity may be more important for vegetative and reproductive**
54 **development than previously anticipated.**

55

56 INTRODUCTION

57 Due to their sessile lifestyle, plants can be exposed to severe adverse environmental stresses,
58 resulting in aberrant DNA replication and loss of genome integrity, both potentially affecting
59 growth and plant survival (Hu et al., 2016; Nisa et al., 2019). To cope with such aberrations,
60 eukaryotic cells activate highly coordinated cellular networks, collectively termed the DNA damage
61 response (DDR), which are crucial for maintaining genome stability (Nisa et al., 2019). DDR
62 activation relies on two phosphatidylinositol 3 kinase (PI3K)-like protein kinases, called Ataxia-
63 telangiectasia mutated (ATM) and ATM and Rad3-related (ATR) (Hu et al., 2016). In general,
64 DNA double-strand breaks (DSBs) activate the ATM kinase, whereas ATR is predominantly
65 activated by single-stranded DNA (ssDNA) and defects in replication fork progression (Maréchal
66 and Zou, 2013). ATM is activated by the MRN complex (MRE11, RAD50, and NBS1) that
67 recognizes DSBs (Nisa et al., 2019); ATR responds to the accumulation of the replication protein A
68 (RPA) at ssDNA sites that is generated in response to any lesion that perturbs replication (Iyer and
69 Rhind, 2017).

70 Remarkably, whereas the upstream kinases ATM and ATR and the proteins that participate
71 directly in the DNA repair mechanisms appear to be largely conserved across eukaryotes, the
72 factors that transduce the DNA damage signal appear to have diverged (Hu et al., 2016; Nikitaki et
73 al., 2018). For instance, plants lack orthologous genes for the canonical signal transducer kinases
74 CHK1/2 and the transcription factor p53 that act downstream of ATM and ATR in mammals
75 (Nikitaki et al., 2018). Instead, Arabidopsis possesses a set of plant-specific proteins, including the
76 SOG1 transcription factor (Yoshiyama et al., 2009; Yoshiyama et al., 2013a) and the
77 SIAMESE/SIAMESE-RELATED (SIM/SMR) family of cyclin-dependent kinase inhibitors (Yi et
78 al., 2014). SOG1 is phosphorylated by ATM in response to DSBs (Yoshiyama et al., 2013b) and
79 can be phosphorylated *in vitro* by ATR (Sjogren et al., 2015). This phosphorylation is crucial for
80 SOG1 activation in response to DSBs (Yoshiyama et al., 2017), representing a direct and immediate
81 connection between DNA damage and the transcriptional activation of DDR genes (Yoshiyama et
82 al., 2009; Bourbousse et al., 2018; Ogita et al., 2018).

83 In contrast to mammals, where disruption of ATR induces embryonic lethality (Brown and
84 Baltimore, 2000; Maréchal and Zou, 2013; Menolfi and Zha, 2020) and ATM mutations lead to
85 developmental defects (Menolfi and Zha, 2020), Arabidopsis *atr* and *atm* knockout mutants do not
86 show any vegetative developmental defect under non-stressed conditions (Garcia et al., 2003;
87 Culligan et al., 2004), although *atm* mutant plants display partial sterility (Garcia et al., 2003). Even
88 the *atr atm* double mutant is viable, but fully infertile due to severe defects during meiosis (Culligan
89 and Britt, 2008). In spite of these discrepancies at the organismal scale, the respective roles of ATM

90 and ATR in DNA damage signalling appear to be conserved between plants and other eukaryotes.
91 Indeed, in Arabidopsis, loss of ATM results in hypersensitivity to genotoxic agents that induce
92 DSBs either directly (e.g. exposure to γ -irradiation) or indirectly during the replication process (e.g.
93 crosslinking agents), as observed in all eukaryotes (Garcia et al., 2003; Culligan et al., 2006;
94 Menolfi and Zha, 2020). Likewise, the Arabidopsis *atr* mutants are hypersensitive to replication-
95 blocking agents (Culligan et al., 2004) , as other eukaryotes (Friedel et al., 2009; Segurado and
96 Tercero, 2009; Jossen and Bermejo, 2013). However, ATR deficiency leads to high sensitivity to
97 DSBs in yeast and mammals (Segurado and Tercero, 2009; Jossen and Bermejo, 2013), whereas
98 Arabidopsis *atr* mutant plants show only a slight sensitivity to ionizing irradiation, suggesting only
99 a minor role of this kinase in the response to DSBs in plants (Culligan et al., 2004; Culligan et al.,
100 2006).

101 The described roles for ATR and ATM in Arabidopsis have been assumed to be conserved
102 in other plants such as crops, but molecular evidence is scarce (Manova and Gruszka, 2015;
103 Szurman-Zubrzycka et al., 2019; Zhang et al., 2020), and some differences may exist between plant
104 species. Indeed, recently, the characterization of both kinases in *Physcomitrella patens* revealed
105 differences with their Arabidopsis orthologs, with PpATR playing a predominant role in the
106 transcriptional response to DSBs, rather than PpATM (Martens et al., 2020) and triggering the
107 formation of stem cells from differentiated tissue in response to DSBs (Gu et al., 2020).

108 So far, the roles of ATR and ATM have not been studied during the development of crop
109 seeds. The maize seed consists of three main compartments: the seed coat or pericarp, of maternal
110 origin, and the embryo and endosperm, the two products of double fertilization (Doll et al., 2017).
111 Endosperm development begins with a triploid (3C) cell formed from the two polar nuclei of the
112 ovule and one sperm cell (Domínguez and Cejudo, 2014). After fertilization, mitotic cell
113 proliferation begins, and at approximately ten to twelve days after pollination (DAP), the
114 endosperm cells transition from a mitotic cell cycle to endoreduplication, resulting in a dramatic
115 increase in nuclear volume and DNA content that peaks at 16 to 20 DAP. Grain filling begins
116 simultaneously through the accumulation of storage compounds, such as starch and proteins,
117 necessary to support seedling growth following germination. During the final stages of seed
118 development, the starchy endosperm undergoes PCD, but these cells and their contents remain
119 intact in the mature grain. The cell death of the starchy endosperm is critical to facilitate the rapid
120 mobilization of the storage reserves for the growth of the germinated embryo. Premature induction
121 of PCD would limit reserve deposition and thus jeopardize germination (Young et al., 1997; Young
122 and Gallie, 2000; Domínguez and Cejudo, 2014).

123 Here, we demonstrate that the functional roles of the ATR and ATM kinases are only
124 partially conserved between Arabidopsis and maize, as exemplified by the accumulation of
125 replication defects in maize ATR-deficient plants and differences in fertility defects between the
126 two species. Moreover, our data reveal a crucial role for the ATR kinase in proper kernel
127 development, playing a pivotal role in repressing premature endocycle onset and cell death of the
128 endosperm.

129

130

131 **RESULTS**

132

133 **Generation of CRISPR/Cas9 Mutants for the Maize *ATR* and *ATM* Genes**

134 Maize orthologs of the Arabidopsis *ATR* and *ATM* genes were initially identified using the PLAZA
135 platform (Van Bel et al., 2018). For the *AtATR* gene (AT5G40820), this resulted in a one-on-one
136 relationship with the Zm00001d014813 gene, encoding a protein with 67.2% sequence similarity.
137 The *ATM* gene (AT3G48190) showed a one-on-one orthology with the maize Zm00001d040166
138 gene, although the encoded protein shares only a 47.7% sequence similarity. While the *AtATM* gene
139 contains 63 exons and is spread over 23 kb, the *ZmATM* gene has 78 exons and is spread over more
140 than 123 kb.

141 With both orthologous genes identified, we designed two single guide RNAs (sgRNAs) to
142 induce mutations in the coding sequence of the maize *ATR* and *ATM* genes using CRISPR/Cas9.
143 We introduced these constructs into immature maize embryos via Agrobacterium-mediated
144 transformation to generate knockouts of the maize *ATR* and *ATM* genes. For each construct, T₀
145 mutant regenerated plants were crossed with B104 wild-type plants. Within the offspring, plants
146 were selected for heterozygosity for the mutation and absence of the Cas9 transgenes. These plants
147 were subsequently self-pollinated to obtain isogenic wild-type and homozygous mutant plants. We
148 selected two independent CRISPR/Cas-induced mutant lines for both genes, named ATR-A and
149 ATR-B, representing *Zmatr* mutants, and ATM-A and ATM-B, representing *Zmatm* mutants. While
150 the ATR-B and ATM-A mutant alleles were caused by an indel that generates a frameshift, ATR-A
151 and ATM-B were deletion mutants of hundreds of base pairs (**Supplemental Figure 1**).

152 **Conserved Role of ZmATR in the Response to Replicative Stress**

153 In all eukaryotes studied so far, ATR is required for responses to replicative stress such as fork
154 stalling, which is associated with hypersensitivity to replication-blocking agents (Friedel et al.,
155 2009; Segurado and Tercero, 2009; Jossen and Bermejo, 2013). The main characteristic of
156 Arabidopsis *atr* mutants is a rapid loss of meristem activity due to inability to slow down the
157 replication process in the presence of stalled replication forks (Culligan et al., 2004). To confirm
158 that maize ATR shares this conserved role, we challenged the two *Zmatr* independent lines and their
159 corresponding wild-type plants with hydroxyurea (HU), which is an inhibitor of ribonucleotide
160 reductase. HU treatment depletes cellular deoxyribonucleotide (dNTP) pools, and thereby induces
161 stalling of replication forks. The sensitivity to DNA stress was determined by measuring root and
162 shoot length after three days of growth within medium supplemented with HU. Although both the
163 wild-type and *Zmatr* mutant roots grew at very similar rates in medium without genotoxin (**Figures**

164 **1A and 1B**), the shoot growth in *Zmatr* mutant lines was clearly 40 to 50% smaller in comparison
165 with their wild-type plants (**Figures 1A and 1C**). When treated with HU, the wild-type root growth
166 was not affected, whereas the *Zmatr* mutant roots were reduced by ~60% in comparison with
167 untreated plants (**Figures 1A and 1B**). A similar effect was observed for *Zmatr* mutant shoot length
168 with a decrease of ~40% compared with ~15-20% in wild-type plants (**Figures 1A and 1C**). As
169 expected, ZmATM is not involved in the stabilization of stalled forks, as the *Zmatm* mutant lines
170 did not display inhibition of growth under treatment nor under control conditions (**Figures 1A, 1D,**
171 **and 1E**).

172 To determine whether the ZmATR and ZmATM kinases are involved in controlling the
173 transcriptional activation induced by replicative stress, we monitored the expression level changes
174 of several DDR-related genes, including the putative maize orthologous genes for *RAD51A*,
175 *RAD51B*, *BRCA1*, *XRI*, *RAD54* involved in homologous recombination (HR), *RAD7A* that
176 participates in nucleotide excision repair, and the *RNR1* and *TSO2* ribonucleotide reductase subunits
177 that function in the synthesis of nucleotides (Roa et al., 2009; Sánchez-Pons et al., 2011; Lahari et
178 al., 2018). To map the rapid transcriptional changes, *Zmatr* and *Zmatm* mutant plants were treated
179 with 5 mM HU for 90 min. For all genes tested, the early replication stress response was ZmATR-
180 dependent (**Supplemental Figure 2**). These results show that ZmATR has a conserved role in the
181 replicative stress response.

182 **ZmATR Has a Predominant Role in the Response to DSBs, Whereas ZmATM Plays a Minor** 183 **Role**

184 To explore the roles of ZmATR and ZmATM in response to DSBs, we evaluated the sensitivity of
185 the corresponding mutants to zeocin, which is a radiomimetic agent that generates mainly DSBs.
186 Unexpectedly, *Zmatr* mutants displayed a pronounced root growth sensitivity to 75 μ M zeocin,
187 showing a reduction of root length of ~60% compared with the untreated plants, whereas wild-type
188 plants did not show a significant reduction of root growth (**Figures 2A and 2B**). Intriguingly, with
189 75 μ M of zeocin, no increased sensitivity was observed for the *Zmatm* mutants compared with wild-
190 type plants, which did show a ~10% reduction in root length (**Figure 2D**). Nevertheless, at zeocin
191 treatment with 150 μ M, a clear difference of reduction in root growth was observed in *Zmatm*
192 mutants compared with wild-type roots. Moreover, under all conditions, we observed a slight
193 inhibition of shoot growth, which was similar between all genotypes examined (**Figures 2C and**
194 **2E**).

195 To confirm these results on DSB sensitivity, we also exposed the seedlings to γ -irradiation,
196 which is known to also induce DSBs. Two-day-old seedlings were treated with a dose of 75 Gy.

197 Root and shoot lengths were measured after four days of recovery. Under these treatment
198 conditions, the *Zmatr* mutant lines clearly were more sensitive to the treatment compared with wild-
199 type plants (**Figures 3A, 3C and 3D**), but no differences were observed for the *Zmatm* mutant
200 (**Figures 3B, 3E and 3F**). To examine whether ZmATR is required to respond to higher levels of
201 DNA damage as observed with zeocin treatment, we irradiated with doses of 250 and 500 Gy. Only
202 at 500 Gy, shoot growth in *Zmatm* was severely affected (**Figures 3B, 3E and 3F**) and most of the
203 shoots showed accumulation of anthocyanins, revealed by purple coloring (**Figure 3B, lowest**
204 **panel**). In summary, our results show that ZmATR plays a crucial role in the DDR triggered by
205 DSBs in maize, as described for yeast and mammals (Cimprich and Cortez, 2008; Blackford and
206 Jackson, 2017), whereas ZmATM contributes to the response under severe DNA-damaging
207 conditions only.

208 Previous studies in Arabidopsis suggested that in comparison with ATM, ATR plays only a
209 minor role in the response to DSBs, because Arabidopsis *atm* mutant plants display an enhanced
210 sensitivity to γ -irradiation, whereas *atr* mutants only show slight sensitivity in comparison with the
211 wild type (Culligan et al., 2004; Culligan et al., 2006). To confirm these observations, we
212 challenged Arabidopsis *atr* and *atm* mutant plants to zeocin and the related drug bleomycin that
213 both generate mainly DSBs. Interestingly, we found that both mutants displayed an increased
214 sensitivity to both DSB-inducing agents in comparison with the wild type (**Supplemental Figures**
215 **3A and 3B**). These results suggest that next to ATM, ATR is also crucial for resistance to DSBs in
216 Arabidopsis.

217 In Arabidopsis, it is known that the ATR and ATM kinases transduce the DNA stress signal
218 to the SOG1 transcription factor, which controls the transcriptional induction of DNA repair genes
219 (Yoshiyama et al., 2013a; Hu et al., 2016; Yoshiyama et al., 2017). We examined in maize whether
220 the transcriptional response to DSBs is affected in *atr* and *atm* mutants. Because γ -irradiation can
221 generate ROS and other types of stresses that lead to the generation of ssDNA (Kim et al., 2019),
222 we only used zeocin to avoid such secondary effects. The same group of genes mentioned above for
223 the response to HU was employed to evaluate the early transcriptional response to zeocin, by
224 harvesting root tips for RT-qPCR analysis after 3-h and 6-h treatment. Wild-type maize plants
225 presented a rapid and strong transcriptional induction to this DNA-damaging agent (**Supplemental**
226 **Figure 2**), as previously reported for Arabidopsis cells (Adachi et al., 2011). The loss of either ATR
227 or ATM impeded the early transcriptional response to DSBs for all the genes evaluated
228 (**Supplemental Figure 2**). These observations appear contrasting with previous observations
229 published for Arabidopsis, where ATR was reported to play only a minor role in the transcriptional
230 response to DSBs (Culligan et al., 2006; Ricaud et al., 2007). A possible explanation is the source

231 of material, being whole Arabidopsis seedlings compared with maize root tips. Therefore, to check
232 whether the role of ATR in response to DSBs differs between maize and Arabidopsis, we decided to
233 evaluate the transcriptional response in the Arabidopsis root tips. Three cyclin-dependent kinase
234 inhibitors (*SMR4*, *SMR5*, and *SMR7*) that are transcriptionally activated by DNA damage (Yi et al.,
235 2014) and DNA repair genes (*RAD51A*, *RAD51B*, *BRCAL*, *XRI-1*, *RAD7A*, *CYCB1;1* and *PARP2*)
236 were included in the analysis. Our results displayed that in *Atatr* root tips the early transcriptional
237 response was attenuated dramatically by zeocin treatment for most of the genes tested, whereas
238 *Atatm* displayed a full loss of transcriptional induction (**Supplemental Figure 4**). These results
239 show that ATR helps to achieve a proper transcriptional induction in response to DSBs in
240 proliferating tissues in both plant species.

241 **Lack of ATR and ATM in Maize Leads to Impaired DNA Repair and Activation of** 242 **Checkpoints in Response to DNA Stress**

243 One essential mechanism to maintain genome integrity is the accumulation of γ H2AX at DNA
244 lesions in an ATM- and ATR-dependent manner (Friesner et al., 2005; Amiard et al., 2010;
245 Maréchal and Zou, 2013; Waterworth et al., 2019). Upon DNA damage, both kinases phosphorylate
246 the histone variant H2AX to generate γ -H2AX foci that recruit repair factors to the break sites
247 (Turinetto and Giachino, 2015; Waterworth et al., 2019). To determine whether the observed
248 sensitivity to DNA-damaging agents of the *Zmatr* and *Zmatm* mutants was associated with the loss
249 of repair capacity and accumulation of DNA damage, we performed immunodetection of γ H2AX
250 foci on root tip nuclei of untreated and treated plants. The number of foci per nucleus varied widely.
251 To visualize the results, we grouped the nuclei population in five categories, depending on the
252 number of foci present per nucleus. Strikingly, all nuclei observed of untreated wild-type plants
253 showed γ H2AX foci (**Figure 4**), indicating the natural occurrence of replication fork collapse
254 during maize genome replication. The *Zmatr-b* and *Zmatm-a* root tips showed a higher number of
255 foci per nucleus compared with its respective wild-type line (**Figures 4A and 4B**).

256 In response to replication stress induced by 24 h exposure to HU, the γ H2AX foci number
257 per nucleus increased in the wild-type ATR and ATM lines, with around 80% of the nuclei showing
258 ≥ 51 γ H2AX foci. *Zmatr-b* mutant nuclei showed a hyperaccumulation of DNA damage foci, with
259 around 49% nuclei presenting ≥ 200 foci, where in the isogenic wild-type line this category
260 represented only 29% (**Figure 4B**). *Zmatm-a* displayed a less dramatic accumulation of foci number
261 per nucleus, with only 42% nuclei showed ≥ 101 γ H2AX foci, while in its wild-type line around
262 57% nuclei were in this category (**Figure 4B**).

263 We also treated the roots for 24 h with zeocin. Strikingly, we observed a hyperaccumulation
264 of γ H2AX foci in *Zmatr-b* mutant nuclei, while the *Zmatm-a* mutant displayed only a slight increase
265 of γ H2AX foci (**Figure 4A**). Indeed, while the wild-type ATR-B and ATM-A nuclei showed
266 around 62% nuclei with ≥ 101 γ H2AX foci, the population of *Zmatm-a* mutant nuclei in this
267 category was 40%. In the case of *Zmatr-b* mutant, almost 80% of nuclei displayed this degree of
268 accumulation of DNA damage foci (**Figure 4B**). These results are consistent with above-mentioned
269 hypersensitivity of *Zmatr* mutants to γ -irradiation and zeocin, which generate mainly DSBs.

270 To know whether *Zmatr* and *Zmatm* mutants are impaired in the activation of cell cycle
271 checkpoints, we examined the cell cycle progression by performing flow cytometry on root tips
272 after 24 h of treatment with HU or zeocin. In untreated root tips, no differences in the proportion of
273 G1, S, and G2 nuclei were observed between the ATR-A wild-type and *Zmatr-a* mutant
274 (**Supplemental Figure 5A**). After 24 h treatment with HU, in wild-type root tips, the population of
275 nuclei in S-phase was enriched as was expected because HU triggers the activation of the intra S-
276 phase checkpoint (Cools et al., 2011). However, in the *Zmatr-a* mutant, the nuclei population that
277 arrested in the S-phase was less than in the wild type, and there was an increase in the fraction of
278 nuclei in G1/S. In contrast, the *Zmatm-a* mutant did not display differences with the wild type in
279 response to HU (**Supplemental Figure 5A**).

280 The profiles of flow cytometry in response to zeocin were less clear and the differences
281 non-significant (**Supplemental Figure 5A**). Therefore, because in other eukaryotes ATM is
282 required for adequate activation of a G2 checkpoint in response to DSBs (Blackford and Jackson,
283 2017), we determined the number of mitotic events per root tip in wild-type ATM-A and mutant
284 *Zmatm-a*. No differences were observed between both lines in untreated root tips (**Supplemental**
285 **Figure 5B**). However, in response to zeocin after 24 h, the wild-type roots showed a drastic
286 decrease in the mitotic figures of 175 in average per untreated root to 44 mitoses per treated root tip,
287 whereas *Zmatm-a* mutant roots displayed an average of 94 per treated root tip (**Supplemental**
288 **Figure 5B**). These results indicate that ZmATM is required for proper activation of a G2
289 checkpoint in response to DSBs generated by zeocin.

290 **The Maize *atr* Mutant Displays Defective Kernel Development**

291 Similar to *Atatr* and *Atatm* mutants, their counterparts in maize are visually indistinguishable from
292 wild-type plants at adult stage when they are grown under optimal greenhouse conditions, despite
293 the fact that *Zmatr* seedlings were smaller in the first days post-germination in vitro. In contrast to
294 *Atatr* plants that are fully fertile (Culligan et al., 2004), both *Zmatr* mutants displayed smaller cobs
295 (**Figure 5A; Supplemental Figure 6A**), with a reduced kernel number per cob (**Figure 5E**),

296 compared with wild-type plants. Intriguingly, although the *Zmatr* cobs appeared to be fully
297 fertilized at early stages post-fertilization (16 and 28 DAP), a small population of kernels displayed
298 an abnormal phenotype, showing a brown and wrinkled appearance (**Figure 5B**). These kernels
299 died before maturity, resulting in gaps in the mature cobs (**Figures 5A; Supplemental Figure 6A**).
300 The *Zmatr* kernels that did reach maturity were smaller in size and weight compared with wild-type
301 kernels (**Figures 5C and 5D**). The *Zmatm* mutant plants did not display defects on fertility (**Figure**
302 **5F**), contrary to what has been reported for *Atatm* mutants, which are semi-sterile (Garcia et al.,
303 2003). The *Zmatm* mutant lines are indistinguishable from wild-type plants in the cob and kernel
304 phenotypes (**Figures 5F and 5G; Supplemental Figure 6B**), number of kernels per cob (**Figure**
305 **5I**), and mature kernel weight (**Figure 5H**).

306 To gain a better insight into the reasons for the apparent lethality shown for some *Zmatr*
307 mutant kernels, we counted the percentage of abnormal kernels per cob. The abnormal kernel
308 phenotype was observed between 5 to 16% (**Supplemental Table 1**), which is not consistent with
309 the expected 25% Mendelian ratio for an embryo lethal mutation, thus rather suggesting a stochastic
310 frequency. Since Arabidopsis ATM is crucial for pollen viability (Garcia et al., 2003), we examined
311 whether the abnormal kernel phenotype may be associated with a defective pollen phenotype
312 through viability staining on pollen from wild-type and *Zmatr* mutant plants. Nearly all the pollen
313 from *Zmatr* mutant plants were viable, similar to pollen of wild-type plants (**Supplemental Figure**
314 **7A**). To investigate the maternal effect, reciprocal backcrosses with B104 wild-type plants were
315 performed. Pollen from wild-type plants were not able to rescue the *Zmatr* mutant cob phenotype.
316 In contrast, *Zmatr* mutant plants used as pollen donor for the wild type resulted in normal cob
317 development (**Supplemental Figure 7B**). These reciprocal crosses hint to a maternal fertility defect
318 in the *Zmatr* plants.

319 **Lack of ZmATR and ZmATM Results in Endogenous DNA Damage in the Embryo**

320 To determine whether lack of ZmATR or ZmATM may lead to the accumulation of DNA damage
321 in the embryo, which is a developmental stage with a high rate of DNA replication and thus
322 potentially sensitive to endogenous replicative stress, we analyzed γ H2AX foci accumulation in
323 embryos at 16 DAP. As observed in root tips, all nuclei of *Zmatr-a* and *Zmatr-b* embryos showed a
324 higher number of foci per nucleus compared with their respective wild-type lines (**Figures 6A and**
325 **6B**). In the *Zmatr* embryo, the majority of nuclei had ≥ 51 foci, being 68.9% for *Zmatr-a* and 80.2%
326 in *Zmatr-b*, while for wild-type lines the percentage of the nuclei with this foci number were 27.6%
327 and 23.0%, respectively (**Figure 6B**). The *Zmatm* mutant embryo nuclei also displayed an increase
328 of foci number, although this was less outspoken compared with the *Zmatr* mutant embryos (**Figure**

329 **6A**). For instance, *Zmatm-a* and *Zmatm-b* nuclei with ≥ 51 γ H2AX foci were 49.5% and 65.7%
330 respectively, whereas their corresponding wild-type lines showed a percentage of 24.5% and 38.7%.
331 The higher accumulation of DNA damage sites within the *Zmatr* embryonic nuclei was reflected by
332 at least 40% of the nuclei analyzed showing ≥ 100 γ H2AX foci compared with their wild-type lines,
333 in which only 2.1 to 2.6% of their nuclei displayed this amount of DNA damage foci. In the *Zmatm*
334 mutant nuclei only between 11.0 to 18.1% of nuclei contained ≥ 100 γ H2AX foci (**Figure 6B**).
335 Thus, these results indicate that lack of ATR leads to a significant accumulation of DNA damage in
336 the embryo. Moreover, although *Zmatm* mutant plants do not show macroscopic differences, they
337 also show increased endogenous DNA damage at least during the embryo development.

338 **Loss of ZmATR Activity Triggers Premature Endoreduplication in the Endosperm**

339 ATR and ATM are relatively more strongly expressed in embryo and endosperm cells of maize,
340 both in mitotic phase and throughout the endoreplication phase (**Supplemental Figure 8**),
341 suggesting that both kinases might have a relevant role during endosperm development. To test
342 whether the expression levels of cell cycle-related genes are affected during endosperm
343 development in the *Zmatr* and *Zmatm* mutants, we analyzed through RT-qPCR the expression at 10,
344 12, 14, 16, and 19 DAP. The expression levels for almost all evaluated genes with exception of
345 *CDK2* were reduced in *Zmatr* endosperm at 19 DAP in comparison with corresponding wild-type
346 endosperm, whereas at earlier time points, the significant differences were variable (**Supplemental**
347 **Figure 9A**). These results suggest that at 19 DAP, most cells of *Zmatr* endosperm exited the mitotic
348 cell cycle. In *Zmatm* endosperm, a slight decrease in the expression of cell cycle-related genes at 14
349 DAP was observed, but at later time points, expression levels recovered to those of wild-type
350 endosperm.

351 Following the exit of the mitotic cell cycle, the endosperm cells undergo endoreplication
352 (Sabelli and Larkins, 2009). To determine the effects of lack of ATR or ATM on the
353 endoreplication process, developing endosperms of at least three independent cobs were analyzed
354 by flow cytometry. Lack of ZmATM did not lead to changes in endoreplication level
355 (**Supplemental Figure 10**). By contrast, the mean ploidy of *Zmatr-a* and *Zmatr-b* endosperm nuclei
356 was significantly increased at 14 DAP relative to wild-type endosperm, and this phenomenon was
357 sustained up to 19 DAP (**Figure 7A**). This increase was attributed to increased frequencies of 12C,
358 24C, and 48C endosperm nuclei in comparison with wild-type endosperm (**Figure 7B**): around 32%
359 of the nuclei in the wild-type endosperm were between 12C and 48C, whereas these classes
360 represented around 40% of nuclei in the *Zmatr* mutants (**Figure 7B**).

361 We next investigated whether lack of ZmATR affected the endoreduplication as
362 consequence of changes in the expression levels of genes associated with DNA replication such as
363 *MINICHROMOSOME (MCM) 2-7 GENE FAMILY* and *PROLIFERATING CELL NUCLEAR*
364 *ANTIGEN (PCNA)*. The transcript levels were measured by RT-qPCR on RNA extracted from wild-
365 type and *Zmatr-b* endosperms at 10, 12, 14, 16, and 19 DAP. Strikingly, reduced expression levels
366 were observed for all evaluated genes at 19 DAP compared with wild-type endosperm
367 (**Supplemental Figure 9B**), contrasting with the increased endoreduplication observed at this
368 developmental time point. This result suggests that the increased occurrence of endoreduplication
369 might be caused by the regulation at post-translational level such as changes of phosphorylation on
370 replisome proteins.

371 **Cell Death Is Enhanced in *ZmATR* Endosperm**

372 Upon completion of endoreduplication, starchy endosperm cells undergo PCD, resulting in
373 extensive DNA degradation (Young and Gallie, 2000). We evaluated whether the pattern and
374 timing of cell death in *Zmatr* and *Zmatm* mutant endosperms were affected. First, the viability of
375 endosperm cells during kernel development was examined by staining fresh sections with Evans
376 blue, a dye that is excluded from living cells with intact plasma membranes, thereby staining only
377 the cytoplasm of non-viable cells (Young et al., 1997). Between 16 and 22 DAP, staining within the
378 central endosperm was more prominent and clearly more extended in *Zmatr* endosperm compared
379 with wild-type endosperm (**Figure 8A**). To quantify these observations, we determined the cell
380 death area (%) per endosperm of at least seven kernels from three different cobs. At the three time
381 points evaluated (16, 19, and 22 DAP), the cell death area (%) was significantly higher in both
382 *Zmatr* mutants in comparison with their respective wild-type lines (**Figure 8B**). In contrast, *Zmatm*
383 mutants did not show differences with their wild-type plants, except for time point 22 DAP in the
384 *Zmatm-b* mutant, for which a significant increase in the cell death area (%) was observed
385 (**Supplemental Figure 11**). However, because this result was not reproducible for the other
386 independent line, it might rather be caused by variability than as a consequence of the lack of ATM.

387 To study further the cell death within *Zmatr* endosperm, we determined the changes of
388 expression of two lytic proteins that accompany the progression of PCD in the root cap, the S1-P1
389 nuclease BFN1 and the aspartic protease PASPA3-2, both known to be expressed in the endosperm
390 of Arabidopsis (Farage-Barhom et al., 2008; Fendrych et al., 2014; Moussu et al., 2017). At 19
391 DAP, the expression of *PASPA3-2* and *BFN1-2* was 1.6- and 2-fold, respectively, higher in *Zmatr*
392 than in wild-type endosperm (**Figure 8C**). Together, these results indicate that lack of ATR leads to
393 more prominent and extended cell death in the endosperm likely by an earlier transition to cell

394 death. Although this phenomenon was observed in viable *Zmatr* kernels, abnormal *Zmatr* kernels
395 presented massive cell death in the whole endosperm at 16 DAP (**Supplemental Figure 12**), which
396 was consistent with the loss of viability of these kernels.

397 To determine whether the increased endoreduplication and early cell death affected starch
398 and storage protein synthesis in the *Zmatr* kernels, we first evaluated the expression of genes
399 involved in the protein (*19KDa zein*) and starch synthesis (*Opaque1*, *Opaque10*, *SS4*, *SSIIa*, and
400 *Shrunken 2*) (He et al., 2019). The expression levels of genes linked to starch synthesis displayed a
401 significant increase of more than 2.5-fold at 19 DAP in *Zmatr-b* endosperm compared with wild-
402 type endosperm (**Supplemental Figure 13A**). Next, we compared starch and protein (non-zein and
403 zein) contents in *Zmatr-b* and wild-type endosperms. While no differences were observed at 19
404 DAP, mature endosperm of *Zmatr-b* kernels showed a significant reduction in the starch and zein
405 protein content (**Supplemental Figures 13C and 13E**), consistent with the smaller size of the
406 *Zmatr* kernels (**Figures 5C**). In *Zmatm* endosperm at 19 DAP, a lower accumulation of starch was
407 found (**Supplemental Figure 13B**), but no difference was observed in mature endosperm
408 (**Supplemental Figure 13C**). Likewise, although *Zmatm* endosperm displayed a significant
409 reduction of starch and protein synthesis-related genes (**Supplemental Figure 13A**), these changes
410 did not affect the final accumulation of these nutrients in mature kernels. Together, our results
411 indicate that lack of ZmATR, but not of ZmATM, leads to early induction of endoreduplication and
412 cell death in starchy endosperm, affecting starch and protein storage, resulting in the reduction of
413 mature kernel size.

414 **The Presence of Either ZmATR or ZmATM Is Essential for Survival**

415 To determine whether the *Zmatr Zmatm* double mutant is viable, we crossed the *Zmatr-b* and
416 *Zmatm-b* single mutants. No progeny with homozygous mutations in both genes were obtained after
417 genotyping 200 seedlings from the F₂ generation and 100 plants from the F₃ generation. To gain
418 more insight into the basis for the apparent lethality associated with the double mutant, the *atr-/-*
419 *atm+/-* and *atr+/- atm-/-* sesquimutant lines, single mutants and wild-type plants were recovered for
420 further analysis during the development. The sesquimutant plants displayed a slight but significant
421 reduction in the plant height in comparison with the single mutants and wild-type lines of adult
422 plants that grew under optimal conditions in the greenhouse (**Figure 9A**).

423 To better understand the basis for the apparent kernel lethality associated with the double
424 mutation, we performed viability staining on pollen from the sesquimutant and single mutant plants.
425 Contrary to single mutants, where no differences in the pollen viability were observed with wild-
426 type plants, part of the pollen of sesquimutant plants was non-viable (**Figure 9B**). Strikingly,

427 despite the sesquimutants displaying a population of non-viable pollen, full cobs were obtained after
428 self-pollination, although the percentage of abnormal kernels was dramatically increased in
429 comparison with the *Zmatr* single mutant (**Figure 9C**). To evaluate whether the phenotype of
430 abnormal kernels is consistent with a Mendelian ratio, we estimated the percentage of abnormal
431 kernels per cob (**Figure 9C**). Interestingly, the kernels with lethal phenotype were between 35 to
432 45%, rather than the 25% that would be expected for a lethality associated uniquely to double
433 mutant kernels; the early death of some *Zmatr* single mutant plus sesquimutant kernels likely
434 contributed to this higher percentage.

435

436

437 DISCUSSION

438 ATR and ATM Signalling Functions Are Largely Conserved Among Arabidopsis and Maize 439 Upon Exposure to DNA-Damaging Agents

440 Maize *atr* mutants show hypersensitivity towards HU, which initially induces stalling of replication
441 forks by depleting cellular deoxyribonucleotide pools, but also results in DSB formation because of
442 fork collapse (Singh and Xu, 2016). We found that the early transcriptional DDR induced by HU
443 was ATR-dependent and that lack of *ZmATR* fails to arrest cells in the S-phase, accompanied by a
444 strong accumulation of γ -H2AX foci that are indicative for DNA break accumulation in response to
445 HU. It suggests that *Zmatr* mutant plants are not able to stabilize the stalled forks, similarly to what
446 is described for other species. Together, these results show that *ZmATR* has a conserved role in the
447 response to replicative stress. Likewise, as observed in Arabidopsis, we found that *ZmATM* plays
448 an important role in the induction of cell cycle arrest after DSB induction, as illustrated by the high
449 frequency of mitotic events observed in *Zmatm* mutants exposed to zeocin.

450 On the other hand, we found that the DSB-induced DDR depends on both ATR and ATM.
451 Maize *atr* mutants show an excessive accumulation of DSBs after treatment with zeocin, to a level
452 similar to what was observed upon exposure to HU, indicating that the loss of ATR-dependent DDR
453 leads to an impairment in DNA damage repair. In contrast, maize *atm* mutants were far less
454 sensitive to DSB-inducing agents than *Zmatr* mutants and did not show a strong level of γ H2AX
455 accumulation when challenged with zeocin. The number of foci was even significantly reduced
456 compared with wild-type nuclei, suggesting that in maize, like in Arabidopsis, ATM plays a more
457 prominent role than ATR in the phosphorylation of γ H2AX (Friesner et al., 2005; Waterworth et al.,
458 2019). Because γ H2Ax has been shown to facilitate HR in both mammals and Arabidopsis
459 (Maréchal and Zou, 2013; Biedermann et al., 2017), we may hypothesize that the absence of ATR
460 leads to replication stress that activates an ATM-dependent increase of γ H2AX foci. Under normal
461 growth conditions, the relatively low levels of DSBs can be repaired by HR, explaining the viability
462 of the *Zmatr* mutant plants. However, when such plants are challenged by exogenous inducers of
463 DSBs, the break repair machinery fails, leading to massive accumulation of DNA damage.
464 Consistent with this idea, it has been observed that mammalian cells deficient for ATR display
465 elevated chromosomal fragmentation after DSB induction due to defects in repair by HR (Wang et
466 al., 2004).

467 ATR and ATM transduce the DNA stress signals to SOG1, whose phosphorylation is
468 crucial for the transcriptional response to DNA damage, including the transcriptional induction of
469 genes needed for the activation of a transient cell cycle arrest and PCD (Yoshiyama et al., 2009;

470 Yoshiyama et al., 2017; Bourbousse et al., 2018; Ogita et al., 2018). We found that the early
471 transcriptional response to DSBs in maize was dependent on ZmATM, as occurs in Arabidopsis
472 (Culligan et al., 2006; Ricaud et al., 2007). Furthermore, in both Arabidopsis and maize, ATR
473 participates in the early transcriptional response to DSBs in root tip meristems. This important role
474 of ATR in the DSB response had probably been overlooked in Arabidopsis due to the use of whole
475 plantlets for the analysis of changes in gene expression, rather than focusing on meristems as we did
476 here. This would suggest that the respective roles of ATM and ATR vary according to the cell type,
477 ATR playing a more crucial role in proliferating cells, in which DNA damage can interfere with the
478 replication process, whereas ATM may be more prominent in differentiated cells. In addition, the
479 relative contribution of ATR appears to be species specific. Indeed, in Arabidopsis *atr* mutants, the
480 transcriptional activation of DDR genes is only dramatically attenuated, whereas in *Zmatr* it is
481 completely absent. Consistently, the relative importance of ATR and ATM for the regulation of the
482 transcriptional response to DSBs has diverged between eukaryotes. In yeast, Tel1/ATM contributes
483 only marginally to direct DSB repair and is of little importance in checkpoint control (Mantiero et
484 al., 2007), playing only a secondary role in signalling pathways (Craven et al., 2002; Jaehnig et al.,
485 2013), whereas these processes are dominated by Mec1/ATR (Gasch et al., 2001; Watson et al.,
486 2004). Likewise, it has been shown for the moss *Physcomitrella patens* that the early transcriptional
487 response induced by bleomycin (DSBs inducer) was largely dependent on ATR and only marginally
488 on ATM (Martens et al., 2020).

489 Although many functions can be compensated between ATR and ATM in diverse
490 eukaryotes (Tomimatsu et al., 2009; Maréchal and Zou, 2013; Menolfi and Zha, 2020), including
491 Arabidopsis (Friesner et al., 2005; Amiard et al., 2010; Roitinger et al., 2015; Waterworth et al.,
492 2019), other roles are non-redundant or performed predominantly by one of the two kinases, and
493 thus lack of any of them leads to developmental defects as a consequence of genetic instability
494 (Murga et al., 2009; Maréchal and Zou, 2013; Menolfi and Zha, 2020). In maize, this partial
495 functional redundancy between the two kinases appears to be conserved: while at the adult
496 vegetative stage, the *Zmatr* and *Zmatm* single mutants are visually indistinguishable from wild-type
497 plants, like their counterparts in Arabidopsis (Garcia et al., 2003; Culligan et al., 2004), the
498 sesquimutant plants display a slight but significant reduction in the stature and the double mutant is
499 lethal, demonstrating that at least one of the kinases is required for an adequate development. This
500 observation contrasts with Arabidopsis, where the *atr atm* double mutant is viable (Culligan and
501 Britt, 2008).

502 **Essential Role of Maize ATR in Proliferating Cells**

503 Contrary to Arabidopsis, where *atr* and *atm* mutant root nuclei do not show spontaneous appearance
504 of γ H2AX (Friesner et al., 2005; Amiard et al., 2010), we found that maize tissues with a high
505 division rate, such as the developing embryo and root tips of *atr* mutants, display an increased
506 presence of the DNA damage marker γ H2AX in comparison with wild-type plants, suggesting that
507 mutants suffer from replicative stress and/or DNA breakages in proliferative tissues. The maize
508 genome is at least 17-fold bigger than the Arabidopsis genome, and contains much more complex
509 repetitive regions (e.g., microsatellites and quasi-palindromic AT-rich repeats) (Haberer et al.,
510 2005; Schnable et al., 2009). These characteristics probably make its genome more prone to
511 replicative stress, implying that ATR plays a more essential role in species with large versus small
512 genomes. Consistent with this hypothesis, *atr* mutant plants have been isolated in barley, whose
513 genome size is of a same order of magnitude as maize, and around 60% of root meristem cells
514 displayed endogenous DNA damage, resulting in plants with reduced size (Szurman-Zubrzycka et
515 al., 2019).

516 **Contrasting Requirements for ATM and ATR During Meiosis and Early Stages of** 517 **Development in Plants**

518 Intriguingly, contrasting requirements in different species have been observed for plant ATM
519 proteins during meiosis: ATM deficiency results in semi-sterility in Arabidopsis and full infertility
520 in rice (Garcia et al., 2003; Zhang et al., 2020), a phenomenon that we did not observe in maize. In
521 Arabidopsis, although ATM deficiency alone impacts meiotic DSB repair leading to partial sterility,
522 the *atr atm* double mutant displays full sterility and accumulation of chromosomal fragmentation,
523 indicating partial functional redundancy between the two proteins during meiosis (Culligan and
524 Britt, 2008). This suggests that, in maize, ATR may function redundantly with ATM in meiotic
525 cells. Consistent with this idea, the maize sesquimutants showed the appearance of non-viable
526 pollen, whereas single mutants did not display differences compared with wild-type plants.
527 However, how ZmATR and ZmATM participate in meiosis and/or female gametophyte
528 development remains to be revealed. Notably, the production of non-viable pollen in the
529 sesquimutants could either be due to meiotic defects or to defects occurring later, during the
530 development of gametophytes.

531 Conversely, whereas lack of ATR does not affect the fertility in Arabidopsis and barley
532 (Culligan et al., 2004; Szurman-Zubrzycka et al., 2019), in maize it resulted in a slight reduction of
533 fertility, as reflected by a smaller cob size, decrease in the number of seeds per cob, and early
534 abortion of some kernels. However, this effect likely relates to severe replicative stress during the

535 early stages of embryo and endosperm development rather than to meiotic defects, since pollen
536 viability was unaffected in *Zmatr* mutants.

537 **ATR Prevents Early Endosperm Endoreplication and Programmed Cell Death**

538 As mentioned above, mutant maize *atr* cobs show the stochastic appearance of abnormal kernels,
539 which is characterized by an early death before maturity. As we observed that lack of ATR activity
540 results in an increase of replicative stress in embryos of viable kernels, we may hypothesize that the
541 viable *Zmatr* kernels achieve to cope properly with the endogenous DNA damage, while the
542 abnormal kernels accumulate higher levels of breakages of DNA and genetic instability, eventually
543 triggering early death of the kernel.

544 In the Arabidopsis root meristem, DSBs trigger cell differentiation, which includes the
545 transition into the endocycle (Adachi et al., 2011). Furthermore, the excessive accumulation of
546 DNA damage activates PCD in meristematic cells when the DNA damage cannot be repaired
547 (Fulcher and Sablowski, 2009; Furukawa et al., 2010). In Arabidopsis, both endoreduplication and
548 PCD are triggered by the perception of DNA damage through ATR and/or ATM (Fulcher and
549 Sablowski, 2009; Furukawa et al., 2010; Adachi et al., 2011). The single mutants display a delay in
550 the induction of PCD, but they do not lose the capacity to activate this process (Furukawa et al.,
551 2010), while the endoduplication activation is not affected (Furukawa et al., 2010; Adachi et al.,
552 2011). By contrast, induction of endoreduplication and PCD are fully compromised in double
553 mutants (Furukawa et al., 2010; Adachi et al., 2011).

554 Considering that endoreduplication and PCD are an intrinsic part of maize endosperm
555 development, and those processes are induced by DSBs in Arabidopsis through an ATM/ATR-
556 dependent pathway, we may hypothesize that during the mitotic division of endosperm cells, lack of
557 ZmATR leads to the accumulation of DSBs that act as a signal driving an early transition into the
558 endocycle. During the subsequent events of DNA replication, even more DNA damage may
559 accumulate, which would lead to a premature onset of PCD.

560 The early onset of endocycle and PCD in *Zmatr* kernels is reminiscent of the early
561 senescence observed in *Atatm* mutants, in which the level of DSBs increases but the DNA repair
562 efficiency decreases, because AtATM represses DSB-induced expression of genes associated with
563 senescence (Li et al., 2020). Consistent with this idea, the endosperm of non-viable *Zmatr* kernels
564 displays an early cell death phenotype. Likewise, the *Zmatr Zmatm* double mutant kernels abort
565 early, indicating that in maize, the two kinases also have partially redundant functions in these
566 mechanisms: ZmATM could be involved but has a minor role, which in its absence can be fully
567 compensated by ZmATR. Furthermore, the elevated expression of both kinases during endosperm

568 development supports the idea that ATM and ATR have a crucial role during the endosperm
569 development in wild-type kernels. Likely both kinases are involved directly in the signaling of
570 DSBs generated by DNA degradation.

571 The viable *Zmatr* kernels display a reduction in the weight and size of mature seeds,
572 accompanied with a decrease in the starch and proteins content as a consequence of an accelerated
573 kernel maturity process in the endosperm triggered by early endoreduplication and PCD. This
574 reduced accumulation of the storage nutrients may jeopardize the germination, which explains the
575 early shoot growth phenotype of the *Zmatr* seedlings, when they still rely on nutrients supplied by
576 the endosperm. However, this delay of growth may also be related with the importance of DDR
577 during the germination of seeds (Waterworth et al., 2015; Waterworth et al., 2016).

578 In summary, we found that the necessity of the ATM and ATR kinases under non-stress
579 conditions appears to be much higher in maize compared with Arabidopsis, with absence of ATR
580 resulting in both vegetative and reproductive phenotypes that are partially offset by ATM. Our data
581 highlight that the mechanisms involved in the maintenance of genome integrity may be more
582 important for plant development than previously anticipated and indirectly suggest that the presence
583 of a non-optimal DDR might severely affect the yield of field-grown crop plants.

584

585

586 METHODS

587 Plant Medium and Growth Conditions

588 Maize seedlings were grown to maturity in soil in a 24°C growth chamber with a 16-h light/8-h
589 dark regime, 55% relative humidity and 300 $\mu\text{mol m}^{-2} \text{s}^{-1}$ photosynthetically active radiation at
590 plant level. For seedling analysis, the maize seeds were germinated using a paper roll system. Seeds
591 were sterilized for 3 min in 100% ethanol, then submerged in 5% NaClO for 30 min, and finally the
592 seeds were rinsed three times with sterilized water. Twelve seeds were spread out over the paper
593 roll, subsequently the roll paper with seeds was transferred to a recipient with liquid 0.5 ×
594 Murashige and Skoog (MS) medium (Basalt Salt Mixture M0221; Duchefa, The Netherlands).

595 Arabidopsis plants were grown *in vitro* under long-day conditions (16-h light/8-h dark,
596 Lumilux Cool White lm, 50 to 70 $\mu\text{mol m}^{-2} \text{s}^{-1}$) at 21°C on solidified medium (half-strength MS
597 (2.151 g/L), 10 g/L sucrose, and 0.5 g/L 2-(N-morpholino) ethanesulfonic acid (MES), adjusted to
598 pH 5.7 with 1 M KOH and 8 or 10 g/L agar). The T-DNA insertion mutant lines *atr-2* and *atm-2*
599 were previously described (Garcia et al., 2003; Culligan et al., 2004). *Arabidopsis thaliana* seeds
600 were sterilized with 5% NaClO for 20 min and subsequent washing with sterile water. To obtain
601 homogeneous germination, the seeds were vernalized for 2 days at 4°C.

602 Vector Construction

603 The CRISPR construct was adapted from Xing et al. (2014). The pBUN411 plasmid was digested
604 by HindIII, leading to two fragments of 2 kb (hereafter called fragment A) and 11.5 kb. The 11.5-kb
605 fragment was further digested with SpeI, resulting in two fragments of 8.5 kb (called fragment B)
606 and 3 kb. The pP+ plasmid was digested with XbaI and HindIII and was ligated to fragments A and
607 B. This resulted in the whole backbone of pBUN411 being replaced by the backbone of pP+,
608 containing a spectinomycin resistance cassette and a more efficient origin of replication. This new
609 vector was called pBUN411-Sp. Using the CRISPR-P *in silico* gRNA design tool (Lei et al., 2014),
610 we selected both for ATR and ATM two possible target sites. Designed primers with the target sites
611 were used to perform PCR on the pCBC-MT1T2 plasmid (Xing et al., 2014), resulting in a
612 fragment containing the desired target sites and the correct sites for ligation into pBUN411-Sp. This
613 was done for both targeted genes. The vector contained the *bar* (bialaphos resistance) marker gene
614 for selection of transformed callus in plants.

615 Maize Transformation and Selection of CRISPR/Cas Lines

616 Immature embryos of the maize B104 inbred line were transformed using *Agrobacterium*
617 *tumefaciens* EHA101 containing the pBUN411-Sp expression constructs. Transformed calli were
618 selected on increasing concentrations of phosphinothricin after which transformed T₀ shoots were
619 regenerated as described before (Coussens et al., 2012). For genotyping, DNA was extracted from
620 transformed T₀ shoot or leaf material in the next generations (approximately 2 cm²) using the
621 Wizard® Genomic DNA purification kit (Promega, WI, USA). We screened T₀ transformants
622 through PCR (primers are listed in Supplemental Table 2), followed by Sanger sequencing to
623 identify CRISPR/Cas9-induced mutations in the targeted genes. The plants were screened for
624 absence of the *bar* marker by ammonium well assay (Coussens et al., 2012), followed by
625 genotyping for the absence of the Cas9 gene construct. Two independent *atm* and *atr* mutants were
626 selected and backcrossed with B104 wild-type plants. These lines were upscaled and screened in F2
627 to obtain wild-type and homozygous mutant plants (*Zmatm* or *Zmatr*) in the same genetic
628 background.

629 **Genotoxic Treatments**

630 Maize seeds were germinated in a paper roll system for 3 days to ensure a straight root orientation.
631 At this time point, seedlings of similar size (2.5.-3.5 cm) were transferred to a falcon tube (50 mL)
632 with liquid 0.5 × MS medium (mock or supplemented with genotoxin) that was used like growth
633 hydroponic system. Treatments were performed with 2.5 mM HU (Sigma-Aldrich, MO, USA) or
634 zeocin (75 μM or 150 μM). After 3 days of treatment, the plantlets were analyzed for root and shoot
635 lengths.

636 For treatment with γ-irradiation, the maize seeds were grown hydroponically using the paper
637 roll system. After 2 days, the seedlings were treated with γ-irradiation using a ¹³⁷Cs source (C.I.S.
638 Bio, Gif sur Yvette, France) at doses of 75, 250 or 500 Gy, and then returned for growth under
639 hydroponic conditions. After 5 days, the root and shoot lengths were measured.

640 To evaluate the sensitivity to genotoxic agents in Arabidopsis, seedlings were grown for 4
641 days on 0.5 × MS and transferred to genotoxin-supplemented medium (5.0 μM zeocin or 0.2 μg/mL
642 bleomycin). After 10 days, the plantlets were analyzed for root length. All the measurements were
643 performed using the ImageJ software package (https://imagej.net/ImageJ_1.x).

644 **RNA Extraction and RT-qPCR**

645 The RNA extractions for maize were performed in pools of ten root tips (1-2 mm) or endosperms of
646 nine independent kernels (three half endosperms per cob of three independent cobs were mixed to
647 perform the RNA extraction). Total RNA was extracted using a Direct-zol RNA MiniPrep Plus kit

648 (Zymo Research, CA, USA). For Arabidopsis experiments, seeds were germinated on control
649 medium on a nylon mesh and transferred 5 d after germination to control medium or medium
650 supplemented with 20 μ M zeocin for the indicated time, after which at least 200 root tips (1-2 mm)
651 were harvested. RNA was isolated with the RNeasy Mini kit (Qiagen, Germany) and was treated
652 on-column with the RQ1 RNase-Free DNase (Promega, WI, USA).

653 RNA quality and concentration were determined by Nanodrop (Thermo Fisher Scientific, MA,
654 USA). The iScript cDNA synthesis kit (Bio-Rad, CA, USA) was used to prepare cDNA from 1 μ g
655 of RNA according to the manufacturer's instructions. Quantitative RT-PCR was performed in a
656 384-well plate on a LightCycler 480 (Roche, Belgium) with SYBR Green I Master mix (Roche,
657 Belgium) in a final volume of 5 μ L and 0.25 μ M primer concentration. Each reaction was done with
658 three technical and three biological repeats. *EF- α* and *18S rRNA* primers were used for
659 normalization of the maize data, while for Arabidopsis three reference genes were used: *EMB2386*,
660 *PAC1* and *RPS26E*. Relative expression values were manually calculated using the $2^{-\Delta\Delta CT}$
661 method. Primers were designed using Primer3Plus ([http://primer3plus.com/cgi-](http://primer3plus.com/cgi-bin/dev/primer3plus.cgi)
662 [bin/dev/primer3plus.cgi](http://primer3plus.com/cgi-bin/dev/primer3plus.cgi)). Primers used for qRT-PCR are listed in Supplemental Table 2.

663 **Immunostaining of γ -H2AX**

664 Root tips of 3-day-old seedlings or embryos of 16 DAP were fixed overnight in 4%
665 paraformaldehyde in a solution of 1x PME (50 mM Pipes pH 6.9, 5 mM MgSO₄, 1 mM EGTA) and
666 then washed three times for 5 min in 1x PME. For one experimental replication, ten root meristems
667 or six embryos were pooled respectively for nucleus isolation. The dissected tissues were chopped
668 in Galbraith's buffer (45 mM MgCl₂, 20 mM MOPS, 30 mM sodium citrate, 0.1% [v/v] Triton X-
669 100, adjusted to pH 7.0 using 1 M NaOH). After filtering through a 50- μ m CellTrics filter and
670 centrifugation under 200 g for 10 min at 4°C, the supernatant was removed. The nuclei were
671 resuspended in 30 μ L nuclei extraction buffer and spread on slides. The samples were left to dry for
672 1 h at room temperature.

673 Immunostaining was performed as described (Amiard et al., 2010), with the following
674 modifications. Each slide was incubated overnight at 4°C with 80 μ L of a rabbit anti-plant γ -H2AX
675 antibody (kindly provided by Charles White, CNRS, Clermont- Ferrand, France) in a 1:600 dilution
676 in fresh blocking buffer (3% BSA in 1x PBS). Slides were washed three times for 5 min in 1x PBS
677 solution and then incubated for 3 h at room temperature in 100 μ L blocking buffer containing Alexa
678 488-conjugated goat anti-rabbit secondary antibody (Molecular Probes, Invitrogen, CA, USA),
679 diluted 1:1000 in fresh blocking buffer. Finally, DNA was counterstained with 2 μ g/mL DAPI for

680 30 min, after which slides were washed in 1x PBS and mounted in mounting medium. Imaging of
681 the nuclei was done using an Olympus FV1000 confocal microscope.

682 **Mitosis Phase Counting**

683 The number of mitotic events per root tip was examined in untreated and treated root tips with
684 150 μ M zeocin. Root tips were fixed overnight in 4% paraformaldehyde in a solution of 1x PME
685 (50 mM Pipes pH 6.9, 5 mM MgSO₄, 1 mM EGTA) and then washed three times for 5 min in 1x
686 PME. Root apices were digested in enzyme mix (1% w/v cellulase, 0.5% w/v cytohelicase, 1% w/v
687 pectolyase in 1x PME) for 2 h at 37°C. After three washes with 1x PME, root apices were squashed
688 gently between the slide and a coverslip, and frozen in liquid nitrogen. Afterwards, the coverslip
689 was removed, and the slides were left to dry for 1 h at room temperature. The slides were stained
690 with 2 μ g/mL DAPI for 30 min, after which slides were washed in 1x PBS and mounted in
691 mounting medium. Imaging of the nuclei was done with an epifluorescence microscope (Axio
692 Imager.Z2.). The number of mitoses were counted by eye.

693 **Pollen Staining**

694 Fresh pollen from tassels was collected in the morning in Carnoy's fixative (60% ethanol, 30%
695 chloroform, 10% acetic acid). Staining was done with a modified Alexander stain as reported by
696 Peterson et al. (2010). The pollen was spread on slides, and then the staining solution was applied.
697 After 10-15 min of incubation, samples were visualized under a microscope (Olympus BX51).
698 Pollen from at least six independent plants was analyzed.

699 **Flow Cytometry**

700 For maize ploidy analysis of roots, seeds were germinated using the paper roll system. Control and
701 treated root tips (1-2 mm) of 3-day-old seedlings were analyzed. For one experimental replication,
702 ten root meristems were analyzed and three replications per treatment were used. The root tips were
703 chopped with a razor blade in 1 mL of Gif nuclei-isolation buffer (45 mM MgCl₂, 30 mM sodium
704 citrate, 60 mM MOPS, 1% (w/v) polyvinylpyrrolidone 10 000, pH 7.2) containing 0.1% (w/v)
705 Triton X-100, supplemented with 5 mM sodium metabisulphite and RNase (5 U/mL). Propidium
706 iodide was added to the filtered supernatants to a final concentration of 50 μ g/mL. The samples
707 were analyzed using a Cyflow SL3 flow cytometer (Partec-Sysmex) with a 532-nm solid state laser
708 (30 mW) excitation and an emission collected after a 590-nm long-pass filter. For cell cycle
709 analysis, we used the algorithm available in the Flomax software.

710 For endosperm analysis, tissue was obtained by removing the seed coat and embryos from
711 each kernel. At least three kernels were analyzed for each plant. Three individual ears were used for
712 flow cytometry analysis. The endosperm was rapidly chopped on a glass Petri dish using a razor
713 blade in 1 mL ice-cold Galbraith's buffer (45 mM MgCl₂, 20 mM MOPS, 30 mM sodium citrate,
714 0.1% [v/v] Triton X-100, adjusted to pH 7.0 using 1 M NaOH). The homogenate was passed
715 through two layers of a 100- μ M nylon mesh and filtered through a 50- μ m CellTrics filter. Then the
716 nuclei were precipitated (200 g, 10 min, 4°C), and the supernatant was removed. The nuclei were
717 suspended in 200 μ L nuclei extraction buffer, after which 1 mL staining buffer was added (Cystain
718 UV Precise P, Sysmex Partec, Germany). The mix was filtered through a 50- μ m CellTrics filter
719 (Sysmex – Partec) and analyzed by the Cyflow MB flow cytometer (Sysmex Partec, Germany). For
720 each sample, at least 10,000 nuclei were collected and analyzed using a logarithmic scale display.
721 The Cyflogic software was used for ploidy measurements. Mean C-values were calculated
722 according to the following equation: [(n₃ X 3) + (n₆ X 6) + (n₁₂ X 12) +]/total number of
723 nuclei, where n₃ = total number of nuclei in the 3C peak, etc.

724 **Evans Blue Staining**

725 Fresh kernels were collected at 19, 22 and 25 DAP for each wild-type and mutant line. Near-median
726 longitudinal hand sections (approximately 3 mm thick) were stained in 0.1% (w/v) Evans blue (C.I
727 23860) for 2 min as reported by Young et al. (1997). Stained sections were washed with water for
728 30 min and photographed. The analyses were carried out from at least seven kernels of three
729 independent cobs for each genotype.

730 **Analysis of Total Protein and Starch Contents**

731 The total protein and starch contents of the kernels were analyzed as described (Zhang et al., 2019),
732 with some modifications. Twenty endosperms of immature (19 DAP) or mature kernels from the
733 same ear were pooled as a single replicate. Three biological replicates were used for the analysis.
734 Flour was obtained by grinding dry endosperm under liquid nitrogen, and then lyophilized
735 overnight.

736 Starch content determination was performed following the method described by instructions of the
737 Total Starch Assay Kit (Catalog: K-TSTA-50A, Megazyme, Australia) based on the use of
738 thermostable α -amylase and amyloglucosidase. Analyses were performed on 100 mg of flour.

739 For the measurement of protein content, approximately 50 mg of flour was used for the
740 content analysis of zein and non-zein proteins. The non-zein proteins were extracted by adding 1
741 mL of the buffer (12.5 mM sodium borate, 5% SDS, 2% 2-mercaptoethanol, proteases inhibitors) to

742 50 mg flour and incubated overnight at 37°C with constant shaking. Subsequently, the samples were
743 centrifugated at 12,000 g at room temperature for 15 min to precipitate debris. Supernatant was
744 collected and absolute ethanol was added to a final concentration of 70%. The samples were
745 incubated at 37°C for 2 h, then centrifugated at 12,000 g for 10 min at room temperature. The
746 supernatant was transferred to a new tube (zein fraction), and then dried in a Speedvac and
747 resuspended in water. The pellet was used to extract non-zein proteins with 1 mL buffer (12.5 mM
748 sodium borate, 5% SDS, 2% 2-mercaptoethano, proteases inhibitors). The mix was incubated at
749 37°C for 2 h, and then centrifugated for 15 min at 12,000 g and room temperature. The pellet was
750 washed twice with 70% ethanol, air-dried, and resuspended in 8 M Urea. Protein quantification was
751 performed with the Compat-Able Protein Assay Preparation Reagent Kit (Catalog: 23215, Thermo
752 Fisher Scientific, MA, USA) and the Pierce BCA Protein Assay Kit (Catalog: 23225, Thermo
753 Fisher Scientific, MA, USA) following manufacturer's manual.

754 **Statistical Analysis**

755 All statistical analyses were performed using the R software (<https://www.r-project.org/>).

756 **Supplemental Data**

757 The following materials are available in the online version of this article.

758 **Supplemental Figure 1.** Map of CRISPR/Cas9 Mutations

759 **Supplemental Figure 2.** Early Transcriptional Response in *Zmatr-b* and *Zmatm-a* Root Tips
760 Treated with HU or Zeocin

761 **Supplemental Figure 3.** *Atatr* and *Atatm* Mutants Display Sensitivity to Zeocin and
762 Bleomycin, Both DSB Inducers

763 **Supplemental Figure 4.** Early Transcriptional Response in *Atatr* and *Atatm* root Tips
764 Treated with Zeocin

765 **Supplemental Figure 5.** *Zmatr* and *Zmatm* Root Tips Display Impaired Checkpoint
766 Activation in Response to DNA Stress

767 **Supplemental Figure 6.** Cob Phenotype of Wild-Type and *ZmATR* and *ZmATM* Mutant
768 Plants

769 **Supplemental Figure 7.** Pollen Viability of *Zmatr* Is Not Affected, but Reciprocal Crosses
770 Indicate a Maternal Defect

771 **Supplemental Figure 8.** Expression Levels of *ZmATR* and *ZmATM* in Different Tissues and
772 During the Endosperm Development in Wild-Type Plants

773 **Supplemental Figure 9.** Expression Levels of Genes Associated with Cell Cycle Regulation
774 and Replication Initiation During the Development of *Zmatm* and/or *Zmatr* Endosperms
775 **Supplemental Figure 10.** Endoreduplication Is Not Affected in *Zmatm* Endosperm
776 **Supplemental Figure 11.** *Zmatm* Endosperm Does Not Display Differences in Cell Death
777 Timing or Abundance
778 **Supplemental Figure 12.** Cell Death in Endosperm of *Zmatr* Aborted Kernels
779 **Supplemental Figure 13.** Starch and Protein Content in *Zmatr* and *Zmatm* Endosperm
780 **Supplemental Table 1.** Percentage of Abnormal Kernels in *Zmatr* Cobs.
781 **Supplemental Table 2.** Primers Used in This Study
782

783 **ACKNOWLEDGMENTS**

784 The authors thank Annick Bleys for help in preparing the manuscript, Charles White (CNRS,
785 Clermont-Ferrand, France) for the γ H2AX antibody, Fernando Guzman-Chavez (University of
786 Cambridge, Plant Sciences Department, UK) for help with the statistical analysis and Jeannine
787 Drouin-Whabi (IPS2, France) for assistance with maize plant sowing and growth. This work was
788 supported by grants of the Research Foundation Flanders (G011420N and G010820N). Ignacio
789 Achon was benefited from a doctoral fellowship “Don Carlos Antonio Lopez” by El Programa
790 Nacional de Becas from Paraguay (BECAL #164/2017).

791 **AUTHOR CONTRIBUTIONS**

792 J.A.P.G., T.E. and L.D.V. conceived and designed the research. J.A.P.G., T.E., I.A., M-U.N.,
793 H.V.d.D. and C.R. performed the experiments. G.C., M.V.L., and L.P. did the maize
794 transformations. J.A.P.G., T.E., I.A., C.R. and L.D.V analyzed data. J.A.P.G. and L.D.V. wrote the
795 article. All authors read, revised, and approved the article.

796

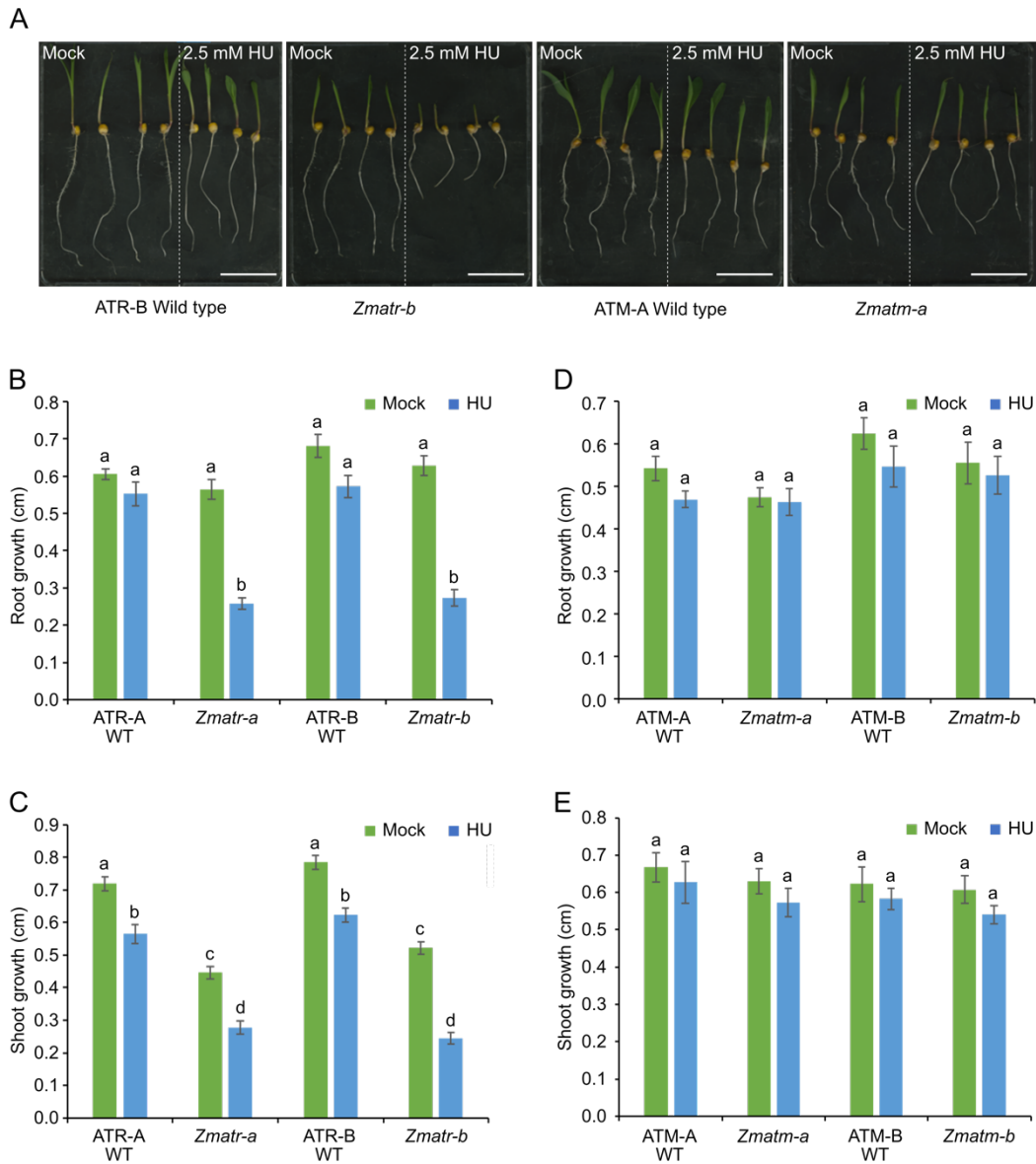


Figure 1. *Zmatr* Plants Are Hypersensitive to Replicative Stress Induced by HU.

(A) Representative wild-type and mutant seedlings following growth for 3 days under control conditions (Mock) or in the presence of 2.5 mM HU. Scale bars = 5.5 cm.

(B and D) Quantification of root growth of ATR **(B)** and ATM **(D)** wild-type and mutant seedlings treated as in **(A)**.

(C and E) Quantification of shoot growth of ATR **(C)** and ATM **(E)** wild-type and mutant seedlings treated as in **(A)**. Letters indicate statistically different growth for each genotype ($P < 0.0001$, mixed model analysis, Tukey correction for multiple testing). Values are average \pm SE; $n = 8-10$.

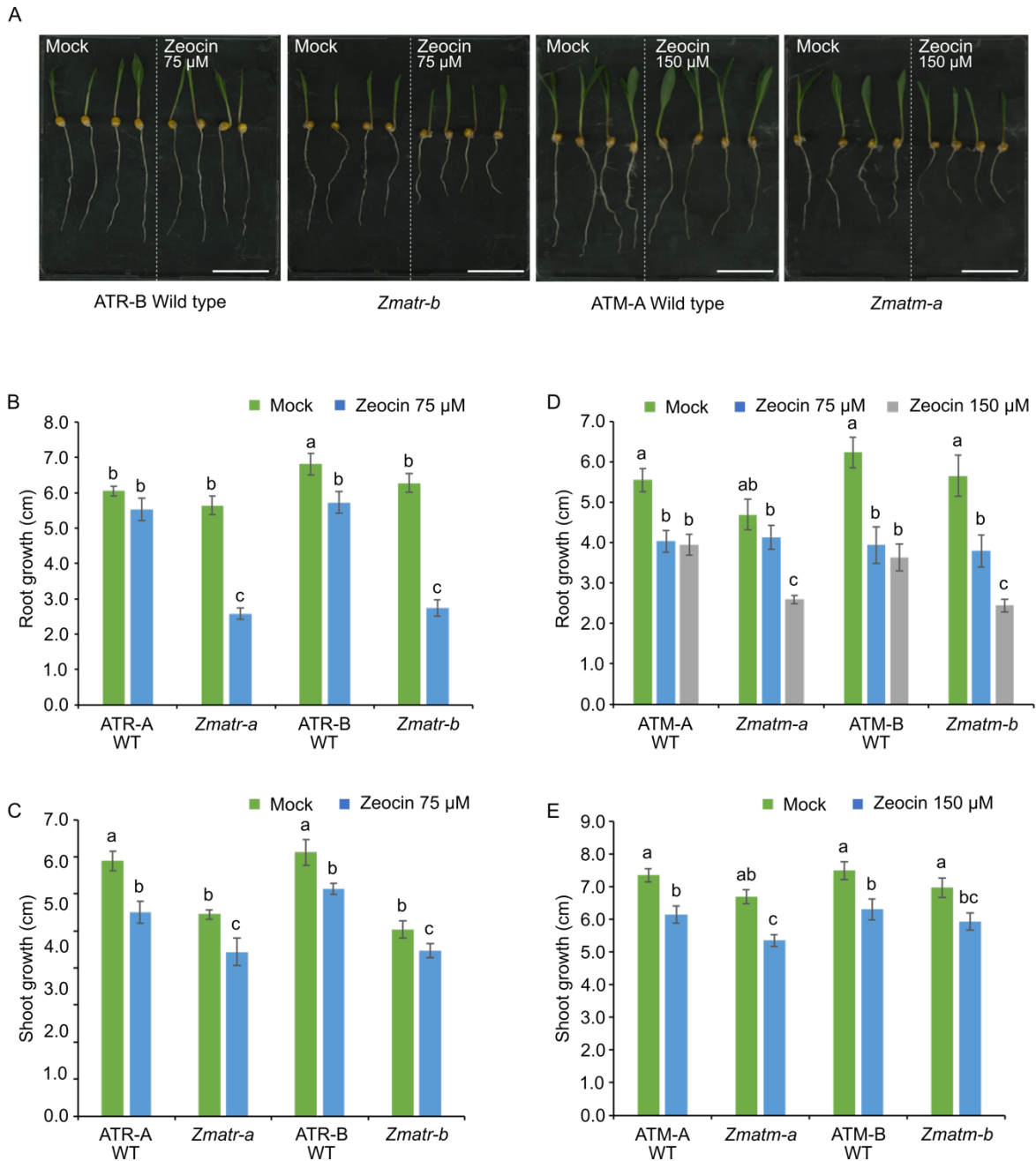


Figure 2. Both Maize ATR and ATM Kinases Are Necessary for Resistance to Zeocin.

(A) Representative wild-type and mutant seedlings following growth for 3 days under control conditions (Mock) or in the presence of 75 or 150 μ M zeocin. Scale bars = 5.5 cm.

(B and D) Quantification of root growth of ATR **(B)** and ATM **(D)** wild-type and mutant seedlings treated as in **(A)**.

(C and E) Quantification of shoot growth of ATR **(C)** and ATM **(E)** wild-type and mutant seedlings treated as in **(A)**. Letters indicate statistically different growth for each genotype ($P < 0.0001$, mixed model analysis, Tukey correction for multiple testing). Values are average \pm SE; $n = 8-10$.

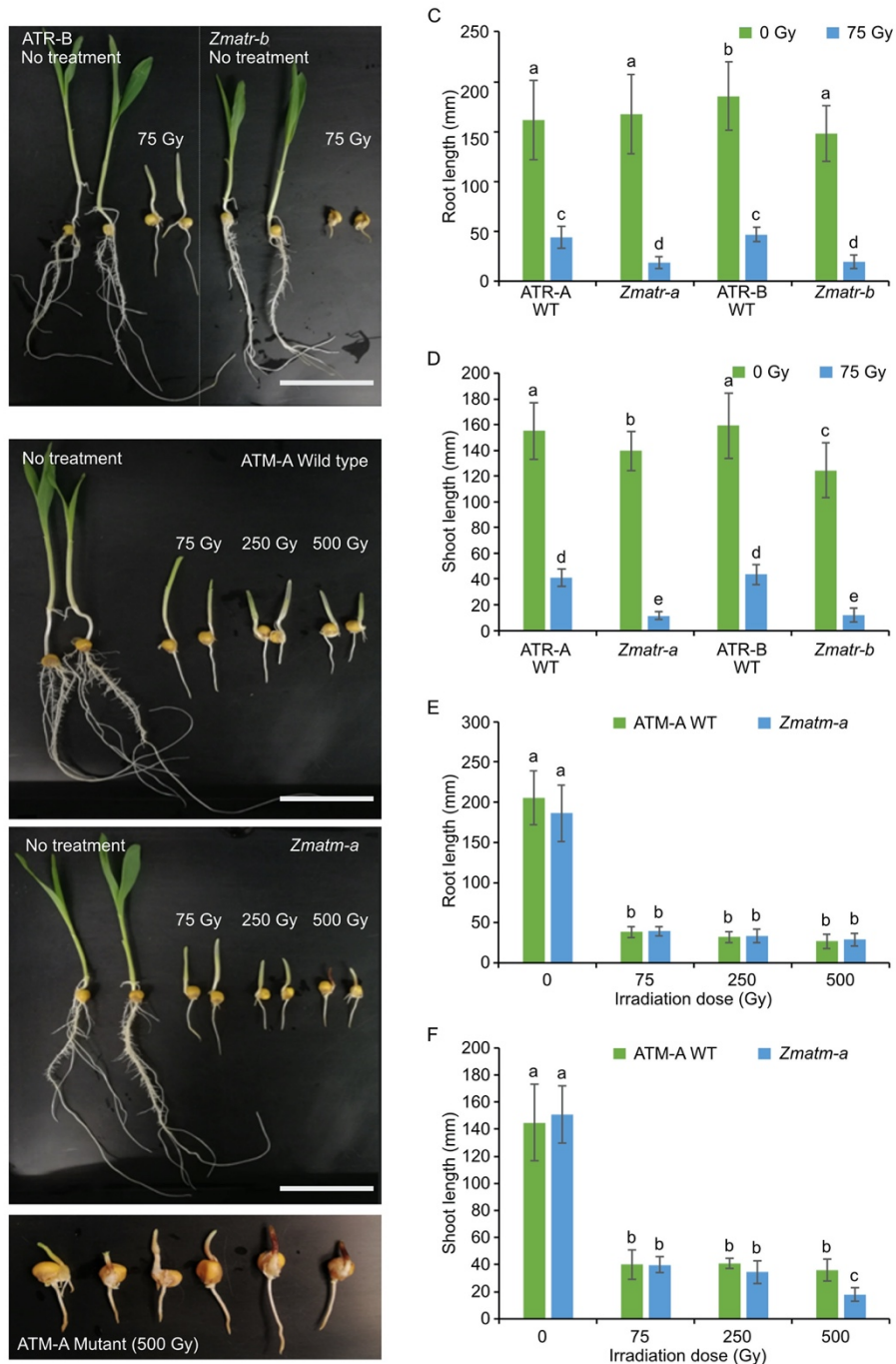


Figure 3. Maize ATR Plays a Predominant Role in the Response to γ -Irradiation-Induced DNA damage.

(A and B) Representative 7-day-old ATR **(A)** and ATM **(B)** wild-type and mutant seedlings grown under control conditions (no treatment) or γ -irradiated at doses of 75, 250 or 500 Gy on day 2. Scale bars = 6.5 cm.

(C and D) Average root **(C)** and shoot **(D)** length of ATR wild-type and mutant seedlings.

(E and F) Average root EC) and shoot (**F**) length in ATM wild-type and mutant seedlings. Letters indicate statistically different growth for each genotype ($P < 0.0001$, mixed model analysis, Tukey correction for multiple testing). Values are average \pm SE; n =26-32.

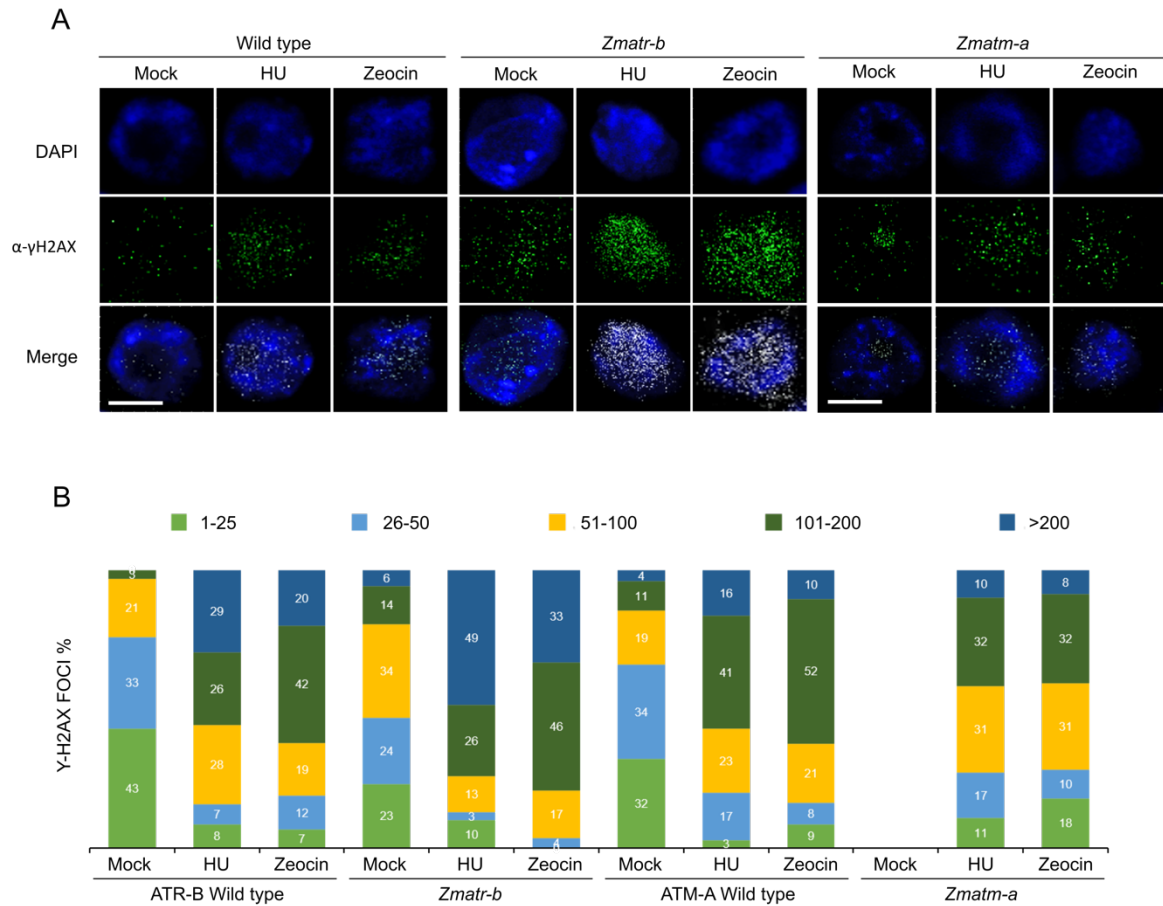


Figure 4. Accumulation of γ H2AX Foci in *Zmatr* and *Zmatm* Root Tips in Response to HU and Zeocin.

(A) Immunostaining of γ H2AX foci accumulation (green) in nuclei stained with DAPI (blue) in maize root tips of wild-type plants and *Zmatr-b* and *Zmatm-a* mutants after 24 h of treatment with 5.0 mM HU or 150 μ M zeocin. Scale bars = 5 μ m.

(B) Quantification of number of γ H2AX foci per nucleus in ATR-B wild-type, ATM-A wild-type, *Zmatr-b* and *Zmatm-a* root tips after 24 h of treatment with HU (5 mM) or zeocin (150 μ M). For each sample, the γ H2AX foci of 100 nuclei were counted and grouped into five categories: 1-25, 26-50, 51-100, 101-200, and more than 200 foci per nucleus.

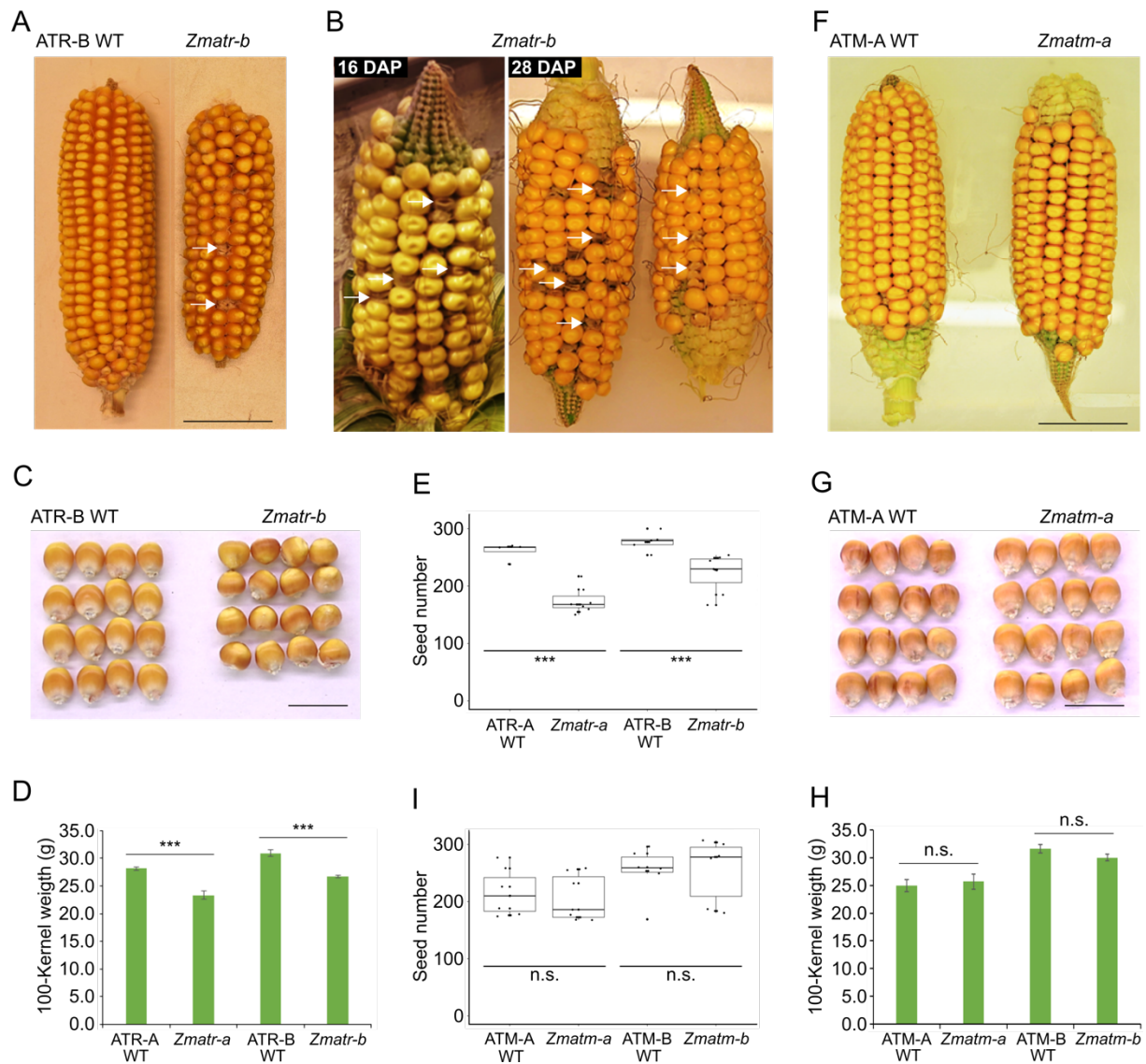


Figure 5. Phenotypic Cobs and Kernels Features of *Zmatr* and *Zmatm* Mutant Plants

(A) Representative mature F₂ ear of wild type (WT) and *Zmatr-b*. Arrows indicate gaps left by early death of kernels. Scale bar = 4 cm.

(B) Representative F₂ ears of *Zmatr-b* at 16 and 28 days after pollination (DAP). Arrows indicate kernels with abnormal phenotype that eventually die.

(C) Representative mature kernels of WT and *Zmatr-b* from a segregated F₂ ear. Scale bar = 1.5 cm.

(D) Comparison of the 100-kernel weight of mature WT and *Zmatr* kernels of two independent lines. Weight was determined in a segregated F₂ population. Values are means \pm SE; n=8-12 (***, P<0.001, Student's *t*-test).

(E) Number of kernels per cob in WT and *Zmatr* plants of two independent lines. Values are means \pm SE; n=7-10 (***, P<0.001, Student's *t*-test).

(F) Representative mature F₂ ear of WT and *Zmatm-a*. Scale bar = 4 cm.

(G) Representative mature kernels of WT and *Zmatm-a* from a segregated F₂ ear. Scale bar = 1.5 cm.

(H) Comparison of the 100-kernel weight of mature WT and *Zmatm* kernels of two independent lines. Weight was determined in a segregated F₂ population. Values are means \pm SE; n=8-9 (n.s., not significant; Student's *t*-test).

(I) Number of kernels per cob in WT and *Zmatm* plants of two independent lines. Values are means \pm SE; n=6-7 (n.s., not significant; Student's *t*-test).

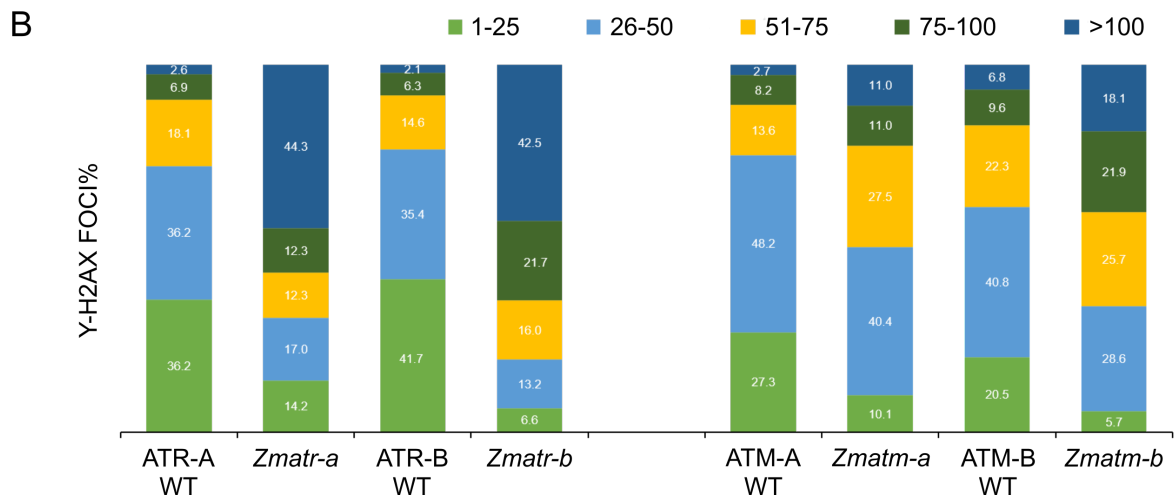
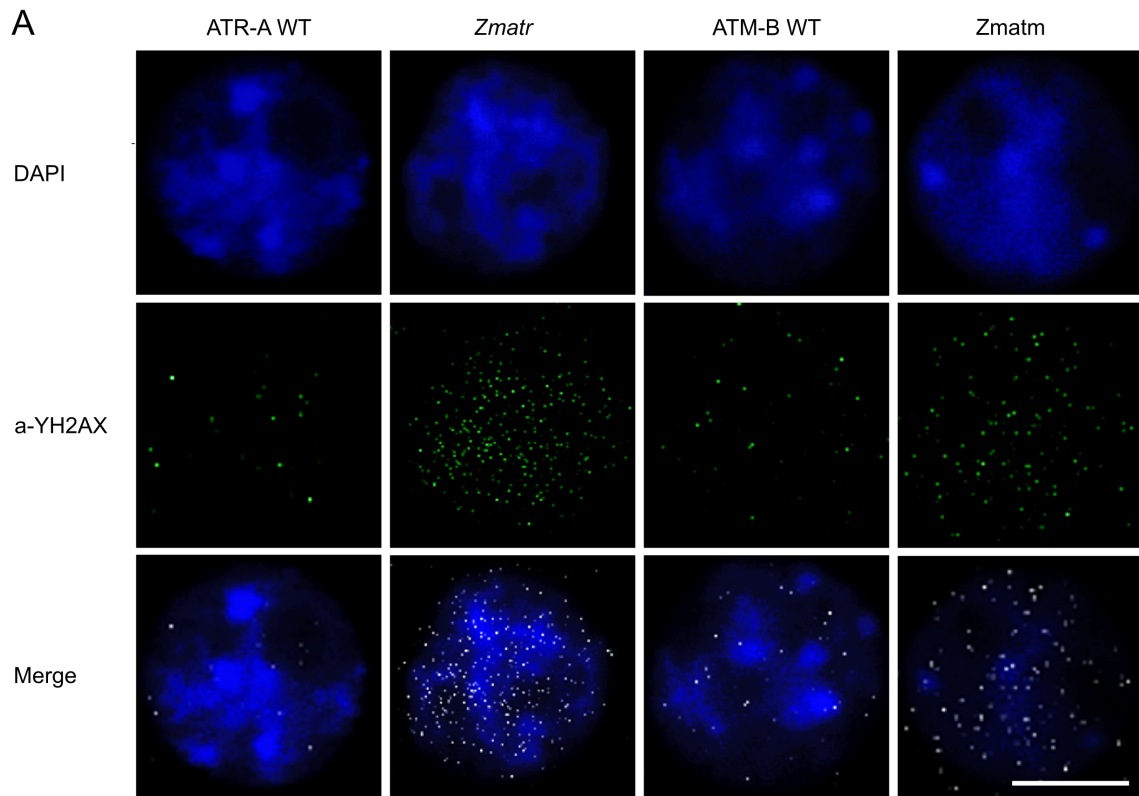


Figure 6. Detection of γ H2AX Foci in *Zmatr* and *Zmatm* Mutant Embryos.

(A) Immunostaining of γ H2AX foci accumulation (green) in nuclei stained with DAPI (blue) of ATR wild-type (WT), *Zmatr*, ATM-WT, and *Zmatm* embryos at 16 days after pollination (DAP). A representative nucleus is shown for each line. Scale bar = 5 μ m.

(B) Quantification of γ H2AX foci in ATR-WT, *Zmatr*, ATM-WT, and *Zmatm* embryos at 16 DAP. For each sample, the γ H2AX foci of 100 nuclei were counted and grouped into five categories: 1-25, 26-50, 51-75, 76-100, and more than 100 foci per nucleus. Two independent lines were analyzed.

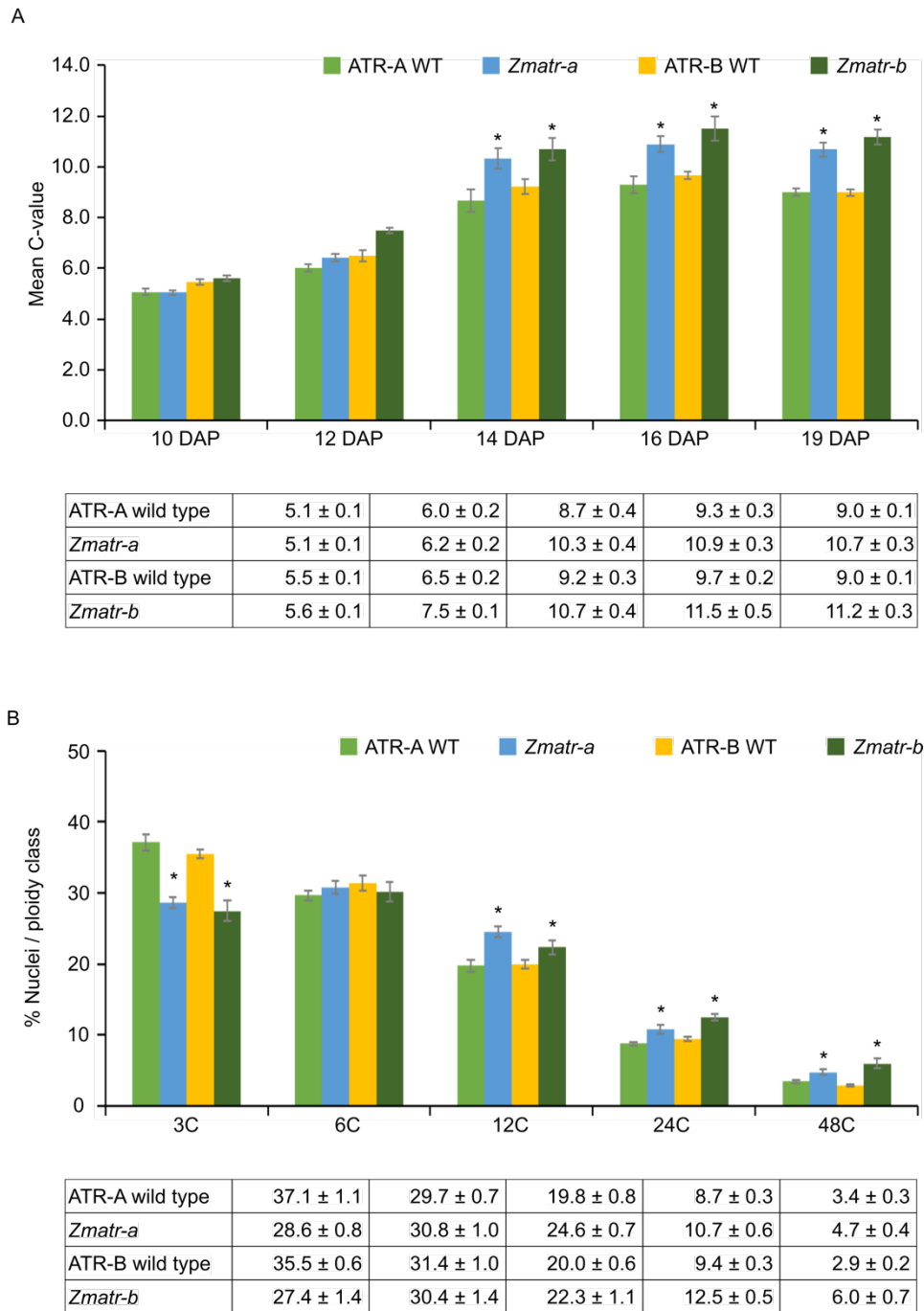


Figure 7. Premature Endocycle Onset in *Zmatr* Endosperm.

(A) The mean C-values in ATR-WT and *Zmatr* endosperm at five developmental stages between 10 and 19 days after pollination (DAP).

(B) Distribution of endosperm nuclei (expressed as a percentage of the total number of nuclei) among different ploidy classes in 19-DAP ATR-WT and *Zmatr* endosperms. Values are means ± SE; n=9-11 (*, P<0.001, Student's *t*-test). All analyses were carried out from at least three kernels of three independent cobs for each genotype.

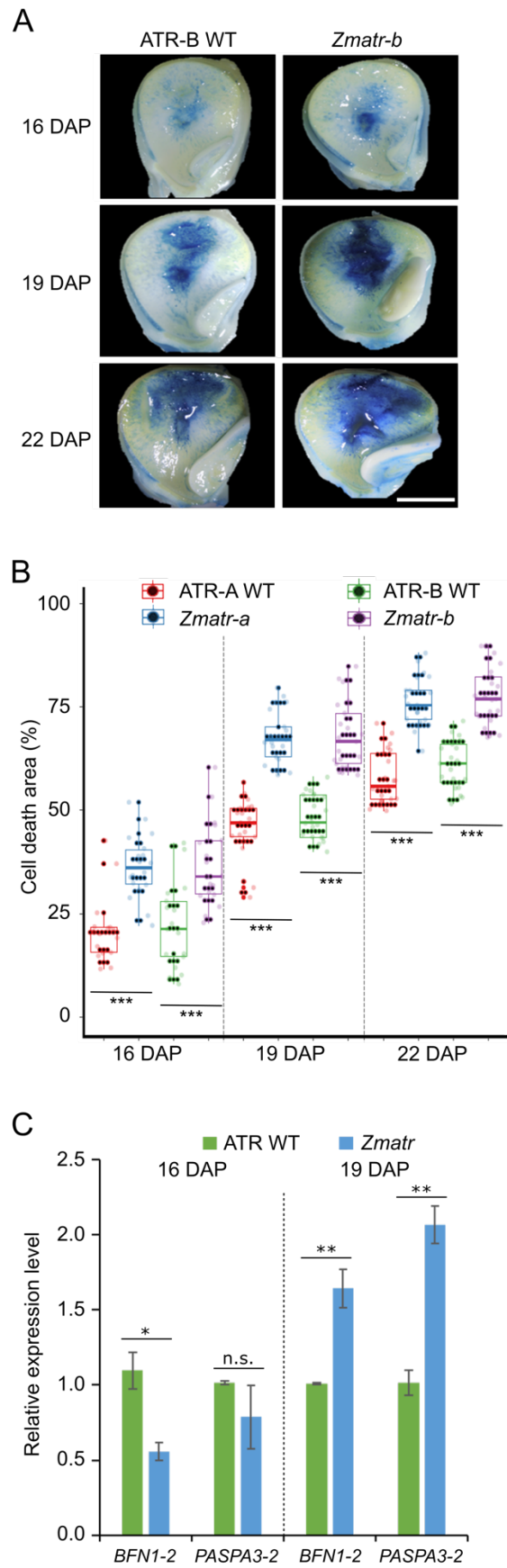


Figure 8. Lack of Maize ATR Results in Enhanced Cell Death in Endosperm.

(A) Progression of endosperm cell death in ATR-B wild-type (WT) and *Zmatr-b* kernels at indicated days after pollination (DAP), as indicated by Evans Blue staining. Dead cells are dark-stained. Scale bar = 3 mm.

(B) Quantification of the percentage of cell death within the endosperm area in ATR-A and ATR-B WT, and *Zmatr-a* and *Zmatr-b* mutants. All analyses carried out from at least seven kernels of three independent cobs for each genotype. Values are means \pm SE; n=21 (***, $P < 0.001$, Student's *t* test).

(C) Expression levels of the *BFN1-2* and *PASPA3-2* transcripts in ATR-B WT and *Zmatr-b* endosperms at 16 and 19 DAP. RNA was extracted of an endosperm pool extracted from at least three kernels of three cobs for each genotype, and the expression levels were measure by quantitative RT-qPCR. Each bar shows the mean \pm SD (** $P < 0.05$; * $P < 0.01$, Student's *t*-test) of three biological replicates.

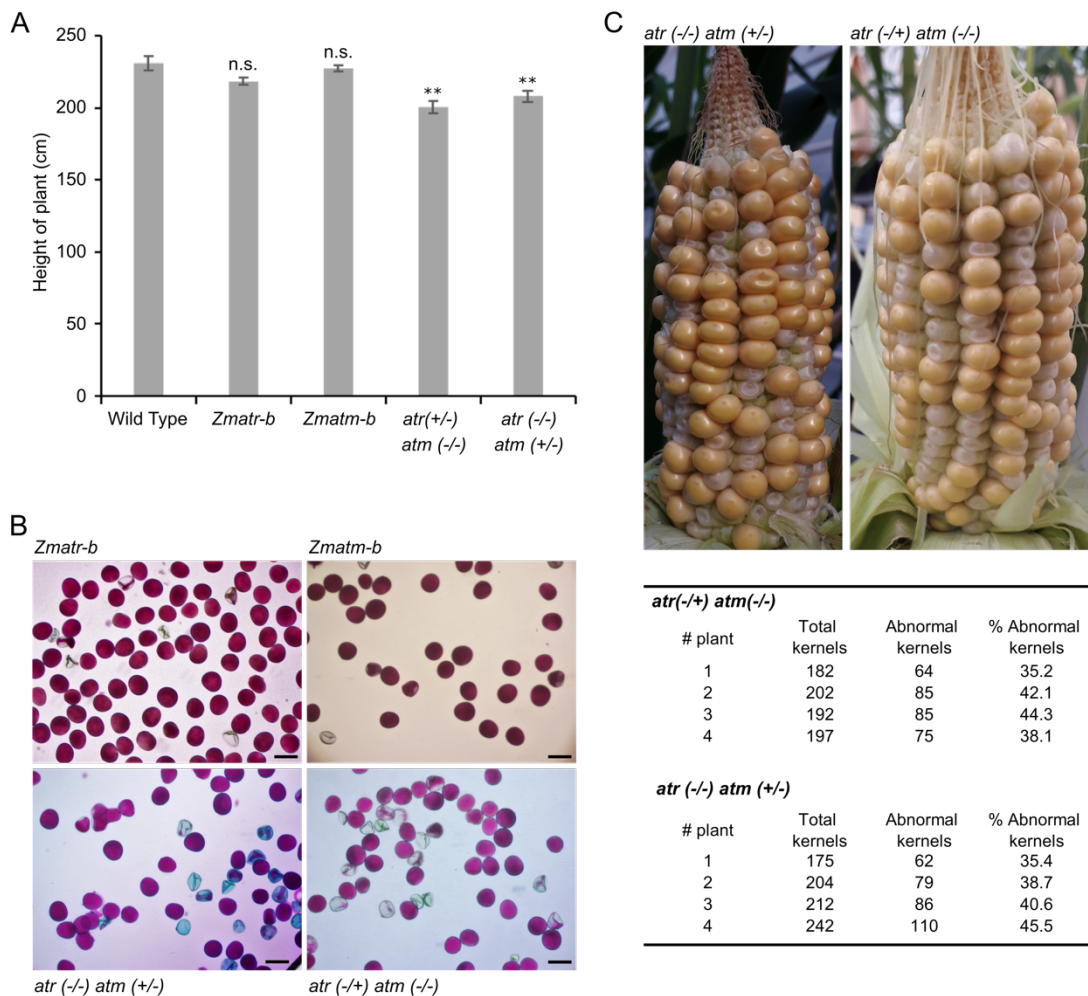
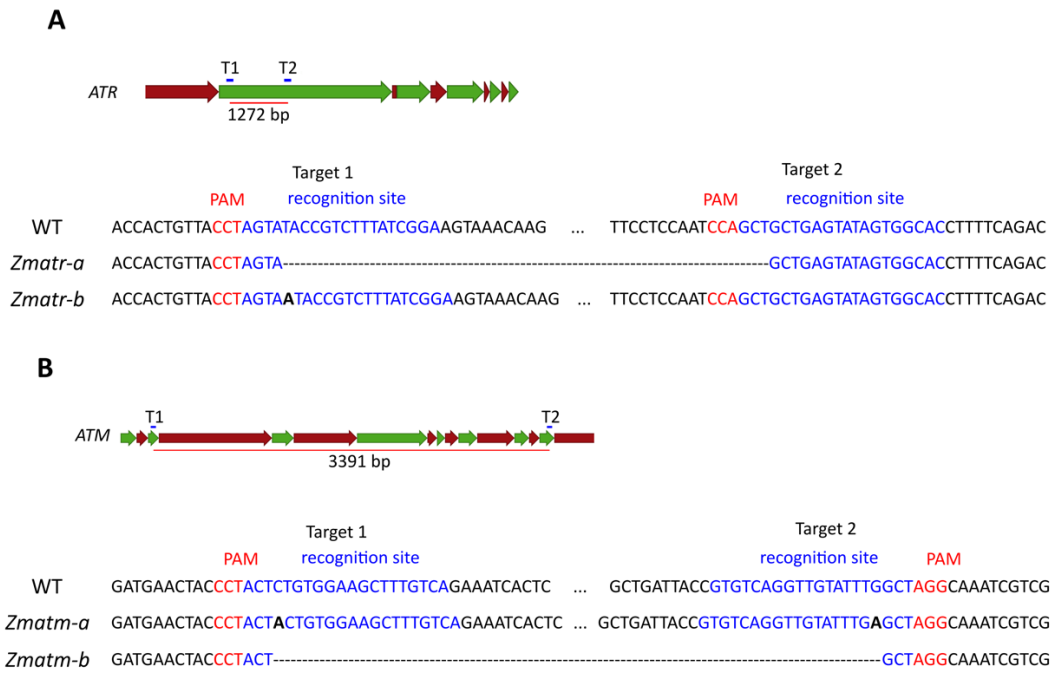


Figure 9. Vegetative and Reproductive Phenotypes of *atm (+/-) atr (-/-)* and *atm (-/-) atr (+/-)* Sesquimutant Plants.

(A) Height of plants (cm) of wild type, *Zmatr-b* and *Zmatm-b* single mutants, and *atm (+/-) atr (-/-)* and *atm (-/-) atr (+/-)* sesquimutants. Height was measured from the soil up to the top tassel. Values are means \pm SE; n=21 (**, $P < 0.005$, Student's *t*-test; n.s = no significant).

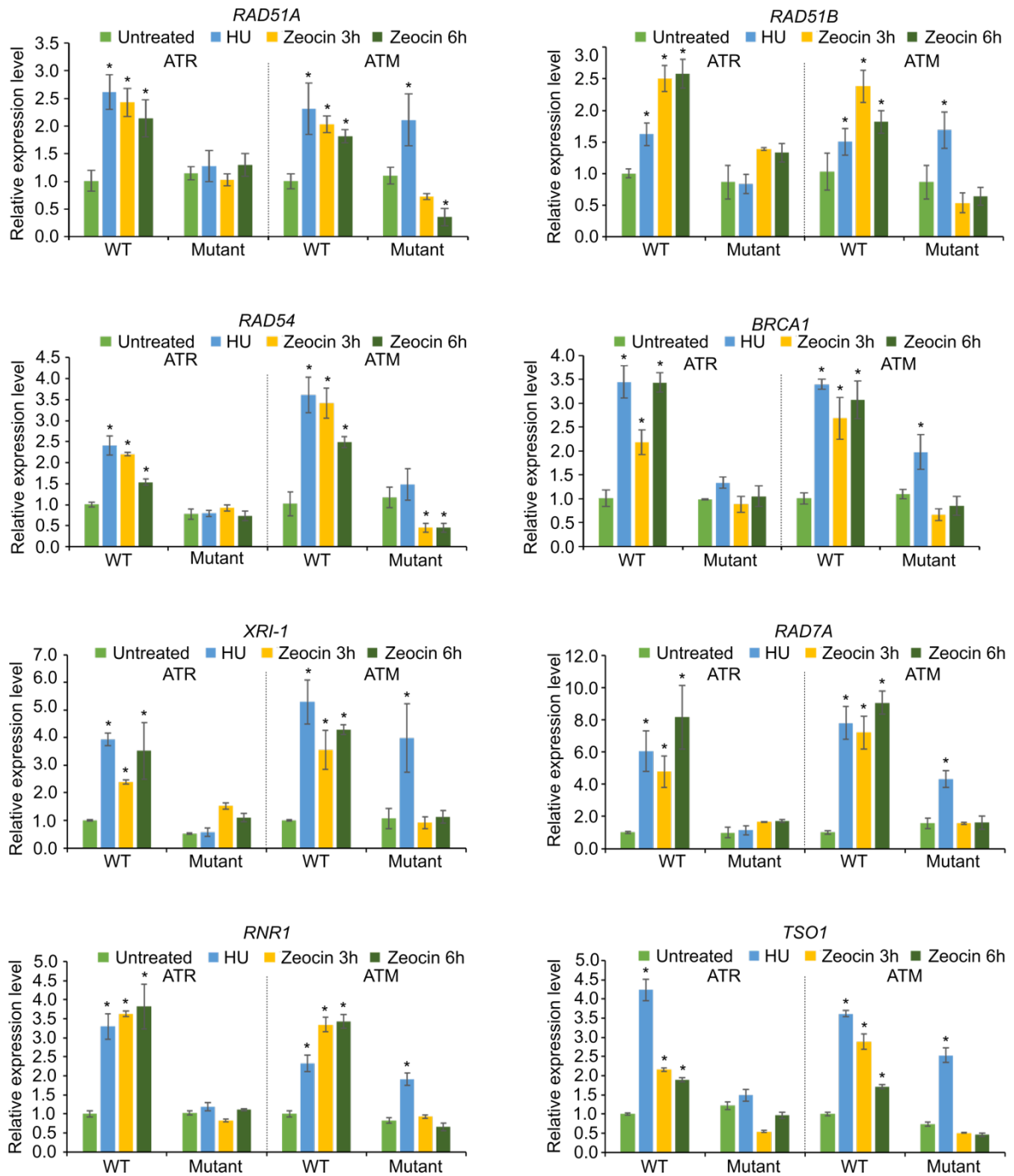
(B) Representative pollen of *Zmatr-b* and *Zmatm-b* single mutants, and *atm (+/-) atr (-/-)* and *atm (-/-) atr (+/-)* sesquimutants. Viability was visualized by Alexander staining. Scale bars = 50 μ m.

(C) Cob phenotype of the *atm (+/-) atr (-/-)* and *atm (-/-) atr (+/-)* sesquimutants at 19 DAP (top panel). Percentage of abnormal kernels per cob of *atm (+/-) atr (-/-)* and *atm (-/-) atr (+/-)* sesquimutants (lower panel).



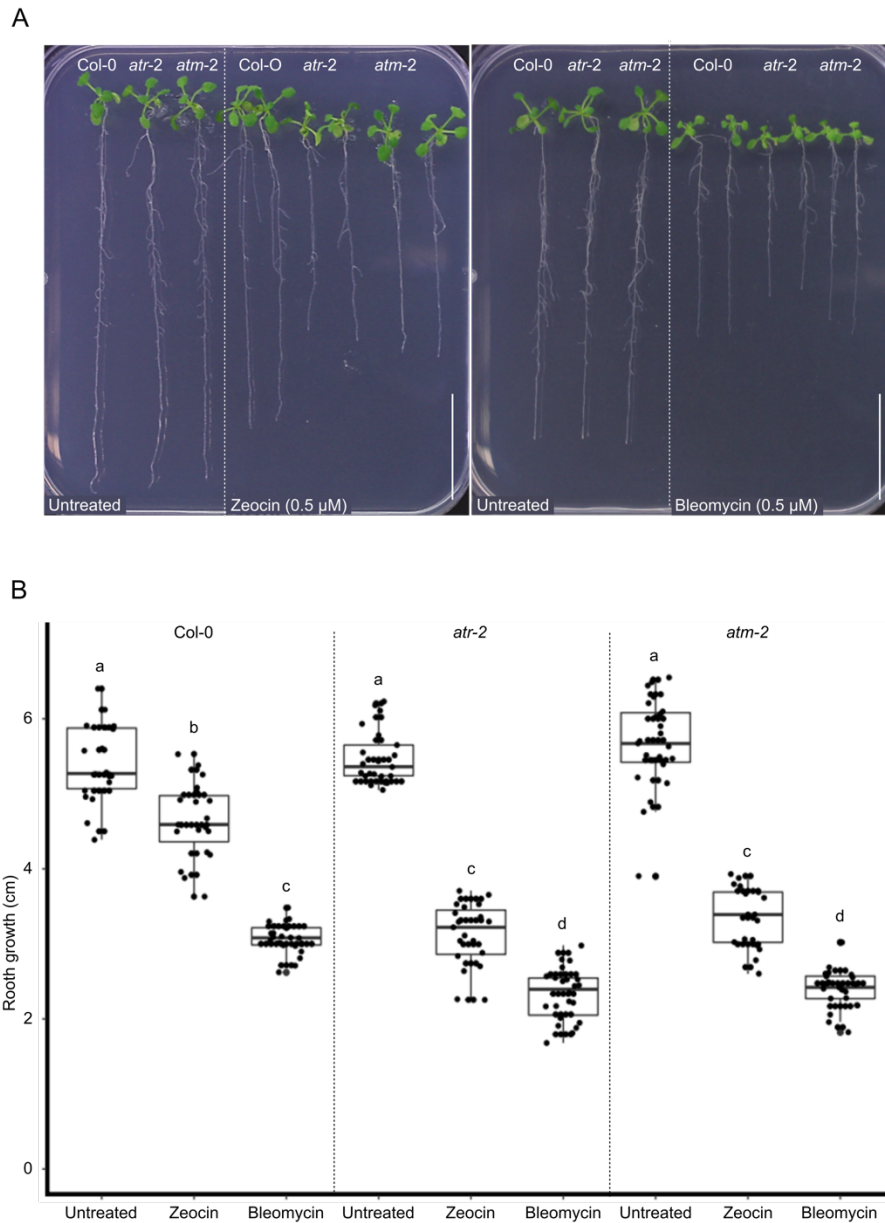
Supplemental Figure 1. Map of CRISPR/Cas9 Mutations (Supports Figures 1 and 2).

Representation of the loci in *ZmATR* (A) and *ZmATM* (B) targeted by the CRISPR/Cas9 construct. Exons are depicted by green arrows, non-coding regions such as introns and untranslated region are depicted by red arrows, gRNA targets are shown as T1 (target 1) and T2 (target 2) above the genes. Red line with number of base pairs underneath the locus indicates the size of deletion if two cuts happen simultaneously. Mutations detected through Sanger sequencing of a fragment PCR-amplified from gDNA. Letters in blue match the gRNA recognition site, letters in red are the PAM sequence. Dashes indicate deletions, bold black nucleotides indicate insertions.



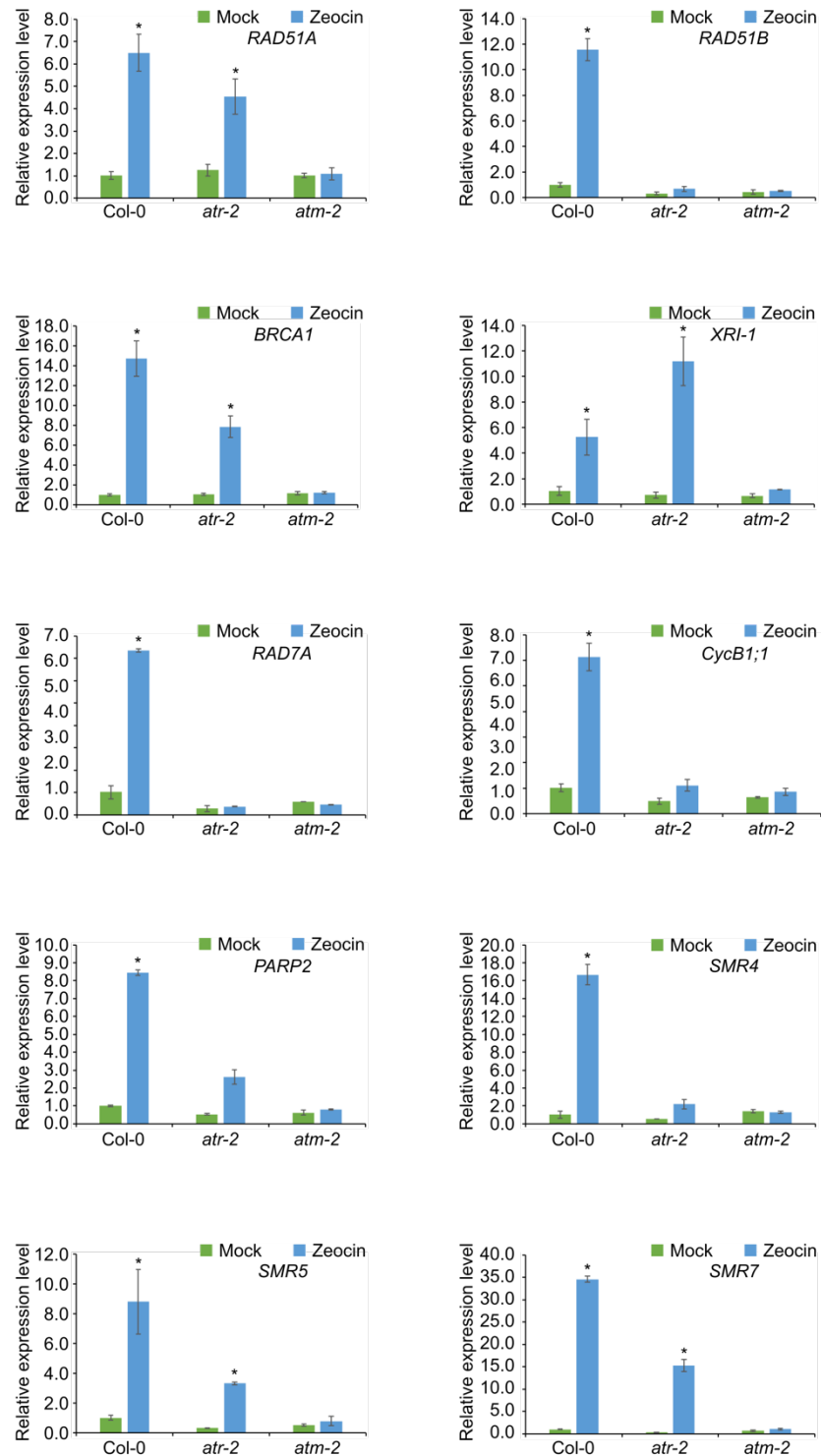
Supplemental Figure 2. Early Transcriptional Response in *Zmatr-b* and *Zmatm-a* Root Tips Treated with HU or Zeocin (Supports Figures 1 and 2).

ATR-B wild type (WT), ATM-A WT, *Zmatr-b*, and *Zmatm-a* seedlings were grown hydroponically for 3 days using the paper roll system. Subsequently, the roots were submerged in 0.5x MS liquid medium (untreated) or supplemented for 90 min with 5 mM HU or 3 h and 6 h with 150 μ M zeocin. RNA was extracted from ten root tips (1-2 mm) and RT-qPCR was performed in cDNA using three biological and three technical repeats. Values are means \pm SE; n = 3 (*P<0.005, Student's *t*-test).



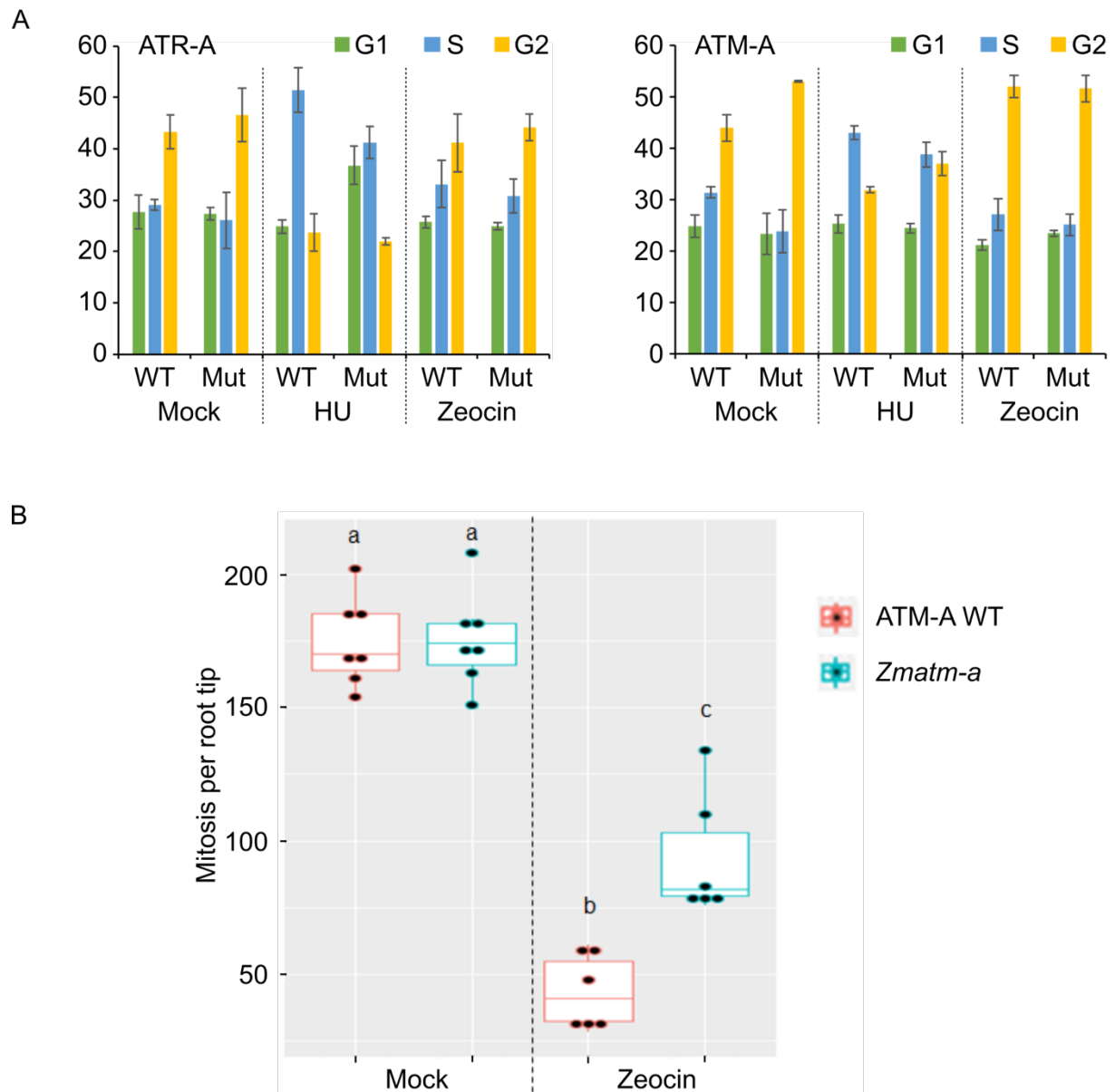
Supplemental Figure 3. *Atatr* and *Atatm* Mutants Display Sensitivity to Zeocin and Bleomycin, Both DSB Inducers (Supports Figure 2).

(A) Representative seedlings of untreated and treated plants. Scale bars = 3.0 cm. (B) Average root length was measured after 10 days ($n \geq 20$ roots for each treatment). Values are average \pm SE. Different letters indicate significantly different values (Student's t -test, $P < 0.05$). Data are representative for two independent experiments.



Supplemental Figure 4. Early Transcriptional Response in *Atatr* and *Atatm* root Tips Treated with Zeocin (Supports Figure 2).

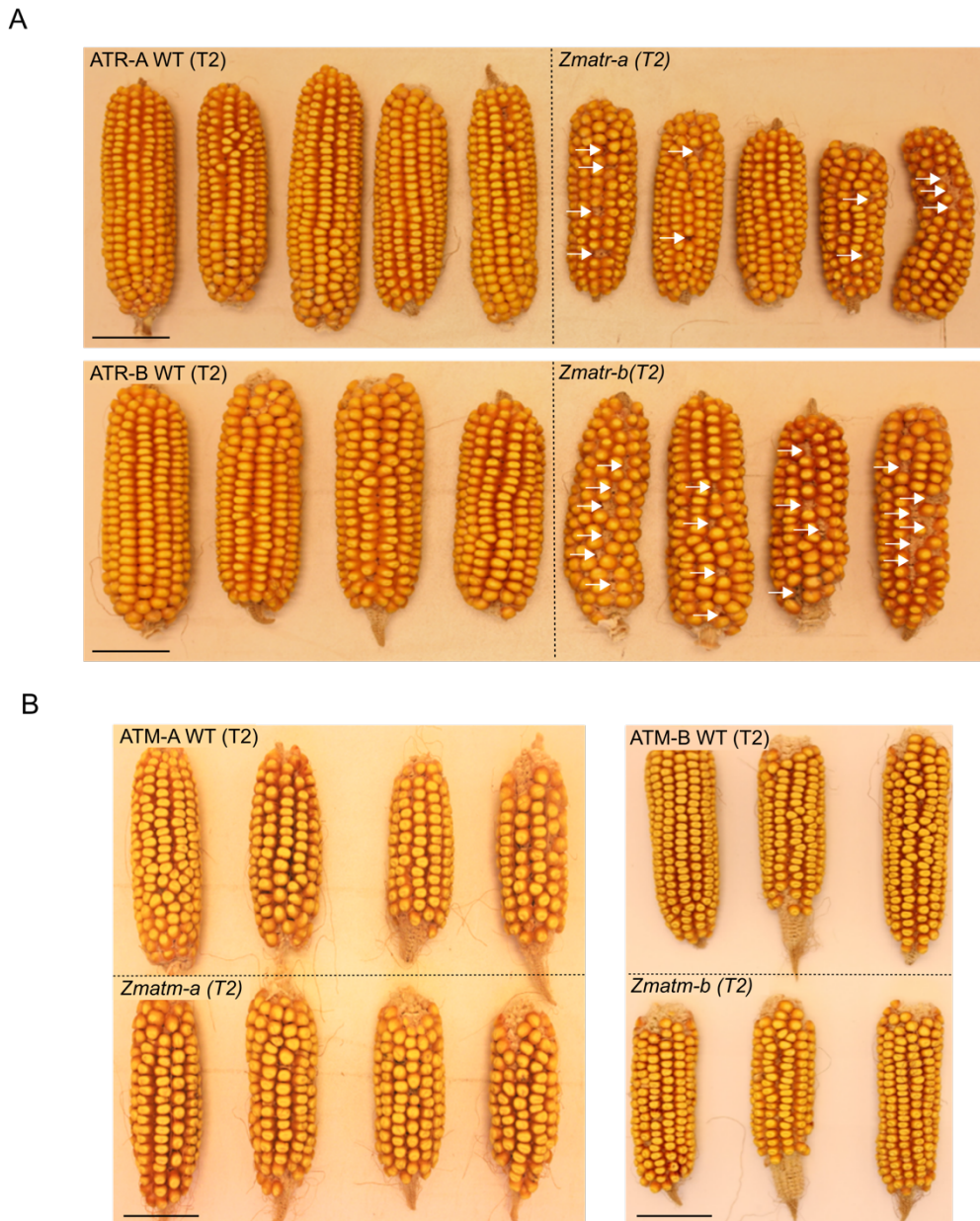
Wild type (Col-0), *Atatr-2*, and *Atatm-2* seedlings were grown for 5 days on 0.5x MS and transferred to genotoxin-supplemented medium (20 μ M zeocin) for 6 h. RNA was extracted from \sim 200 root tips (1-2 mm) for RT-qPCR analysis using three biological and three technical repeats. Values are means \pm SE; n = 3 (*P<0.005, Student's *t*-test).



Supplemental Figure 5. *Zmatr* and *Zmatm* Root Tips Display Impaired Checkpoint Activation in Response to DNA Stress (Supports Figure 4).

(A) Flow cytometry analysis of untreated (mock) and treated root tips of ATR-A wild type (WT), *Zmatr-a* (Mut), ATM-A WT and *Zmatm-a* seedlings. Seedlings were grown hydroponically for 3 days using the paper roll system, after which the roots were treated with 5 mM HU or 150 μ M zeocin for 24 h. The proportion of nuclei in G1, S, and G2 is indicated in the graphs. Data are representative of ten independent observations. Values are means \pm SE; n = 3.

(B) Number of cells in mitosis per root tip in untreated and treated (150 μ M zeocin for 24 h) ATM-A WT and *Zmatm-a* seedlings. Values are means \pm SE; n=6-7 (*P<0.001, Student's *t*-test).

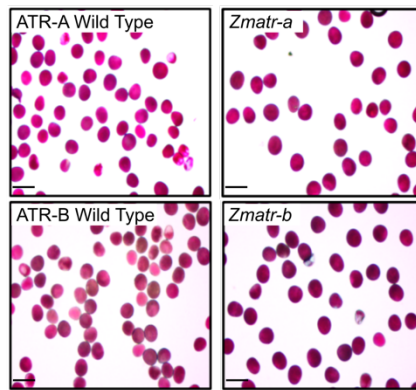


Supplemental Figure 6. Cob Phenotype of Wild-Type and *ZmATR* and *ZmATM* Mutant Plants (Supports Figure 5).

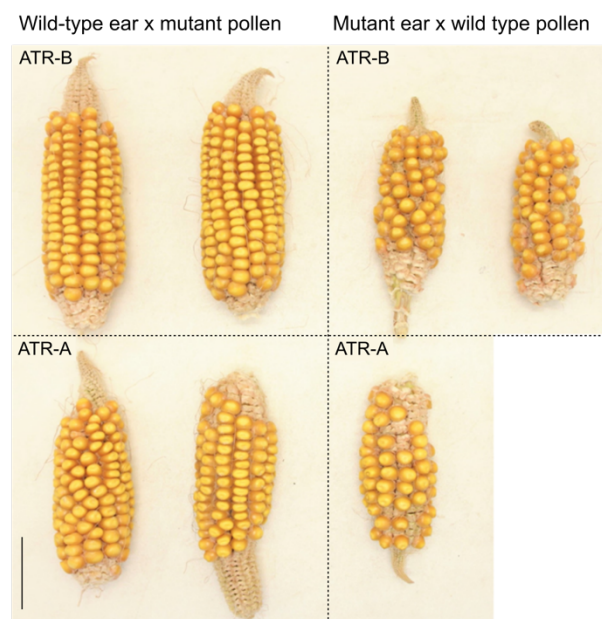
(A) Representative F₂ cobs of ATR-A and ATR-B wild-type plants, and *Zmatr-a* and *Zmatr-b* mutants. Arrows indicate gaps left by early death of kernels. Scale bars = 4 cm.

(B) Representative F₂ cobs of ATM-A and ATM-B wild-type plants, and *Zmatm-a* and *Zmatm-b* mutants. Scale bars = 4 cm.

A



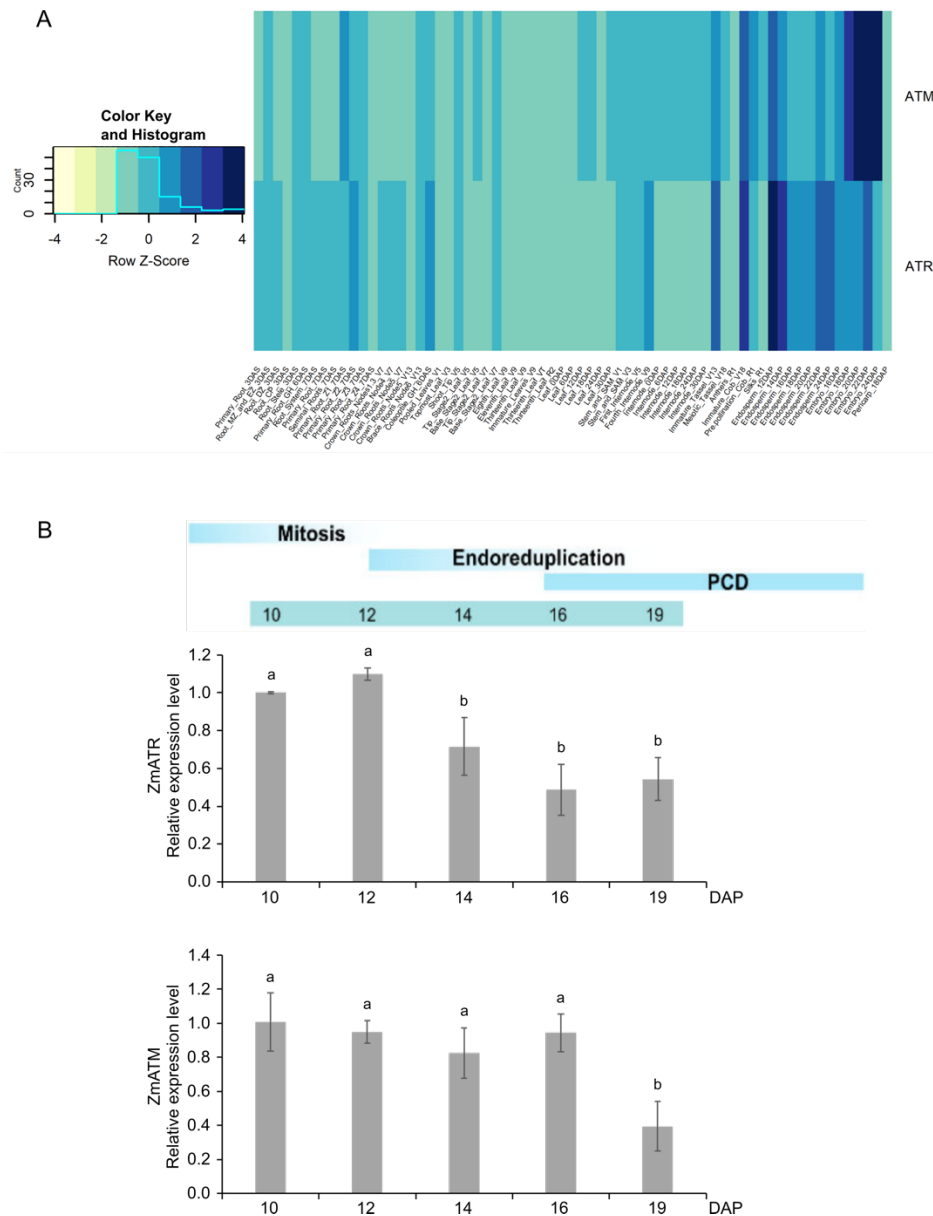
B



Supplemental Figure 7. Pollen Viability of *Zmatr* Is Not Affected, but Reciprocal Crosses Indicate a Maternal Defect (Supports Figure 5).

(A) Alexander staining on ATR wild-type and *Zmatr* pollen. Scale bars = 50 μ m.

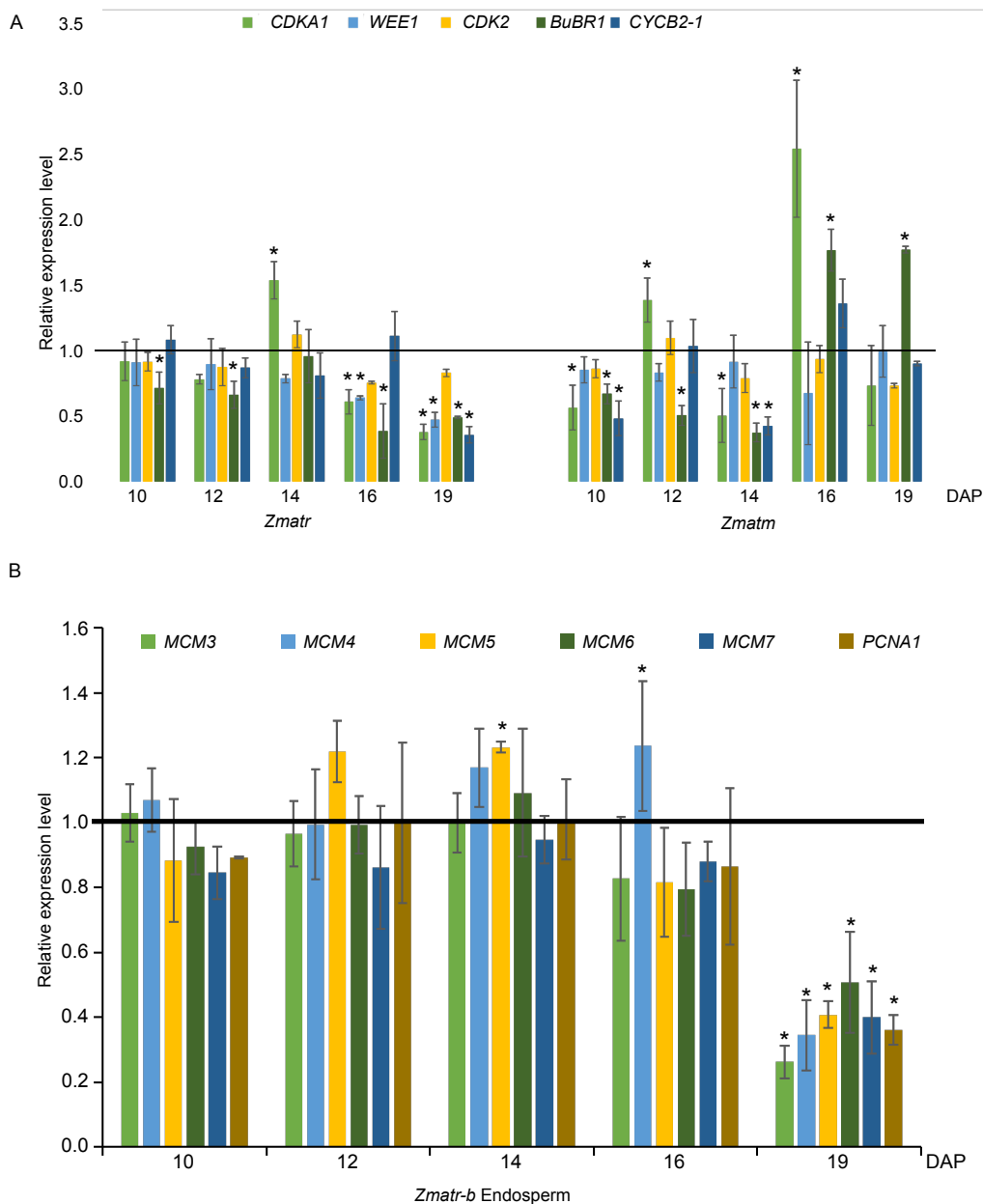
(B) Mature ears of reciprocal crosses. Scale bar = 4 cm.



Supplemental Figure 8. Expression Levels of *ZmATR* and *ZmATM* in Different Tissues and During the Endosperm Development in Wild-Type Plants (Supports Figures 5 and 6).

(A) Heatmap of expression levels for the *ZmATR* and *ZmATM* genes in different tissues in wild-type plants. Expression values were extracted from Stelpflug et al. (2016) and were normalized per row to obtain Z-scores. Heat map was generated by scaling Z-scores per sample.

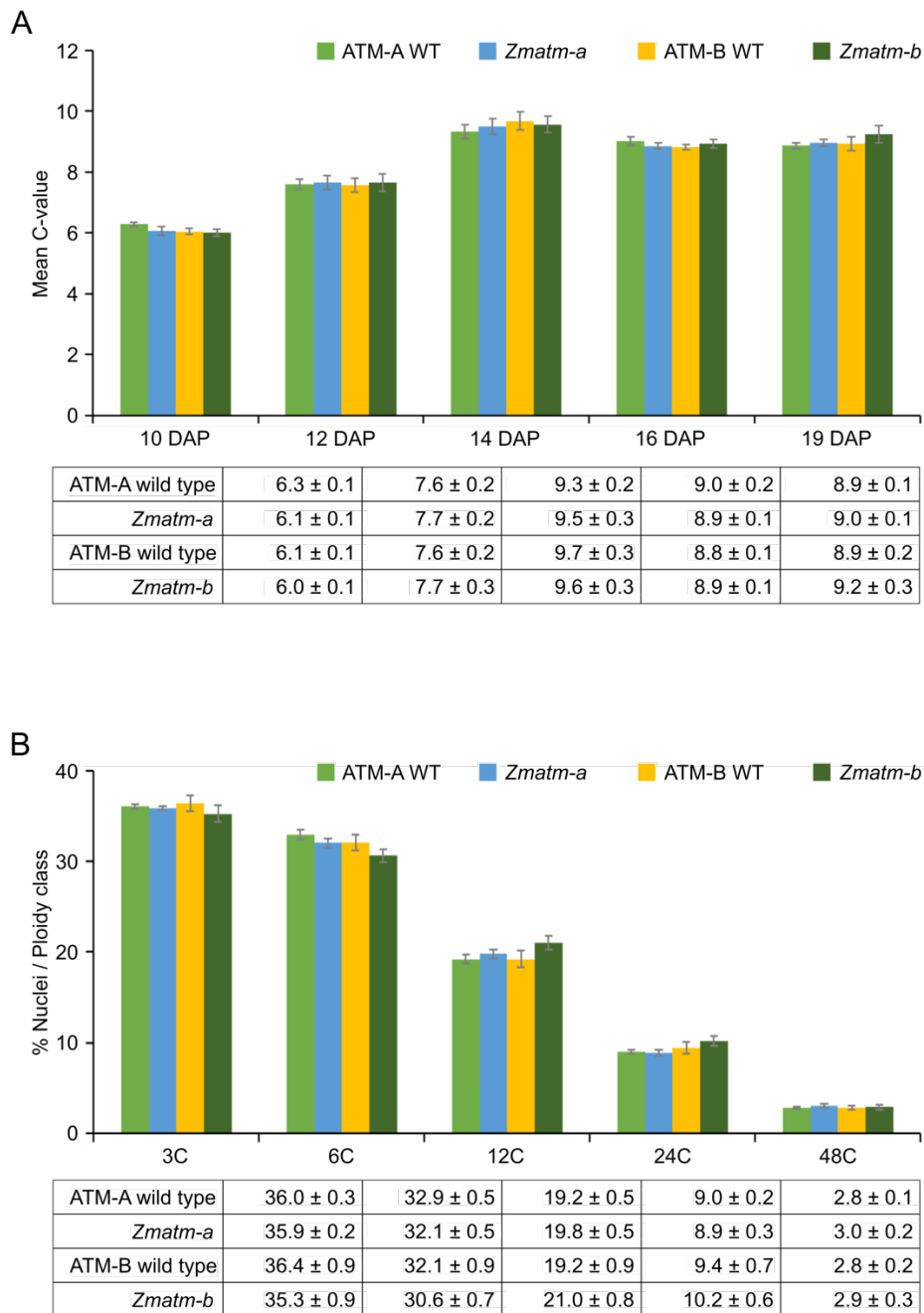
(B) Expression levels of *ZmATR* and *ZmATM* in wild-type endosperm. RNA was extracted at the indicated days after pollination (DAP) of an endosperm pool extracted of at least three kernels of three cobs, and mRNAs were measured by RT-qPCR. Each bar shows the mean \pm SD of three biological replicates. Different letters indicate significantly different values. ($p < 0.001$, mixed model analysis, Tukey correction for multiple testing).



Supplemental Figure 9. Expression Levels of Genes Associated with Cell Cycle Regulation and Replication Initiation During the Development of *Zmatr* and/or *Zmatr* Endosperms (Supports Figure 5 and 6).

(A) Expression levels of cell cycle regulation-related genes in *Zmatr-b* and *Zmatm-a* endosperm.

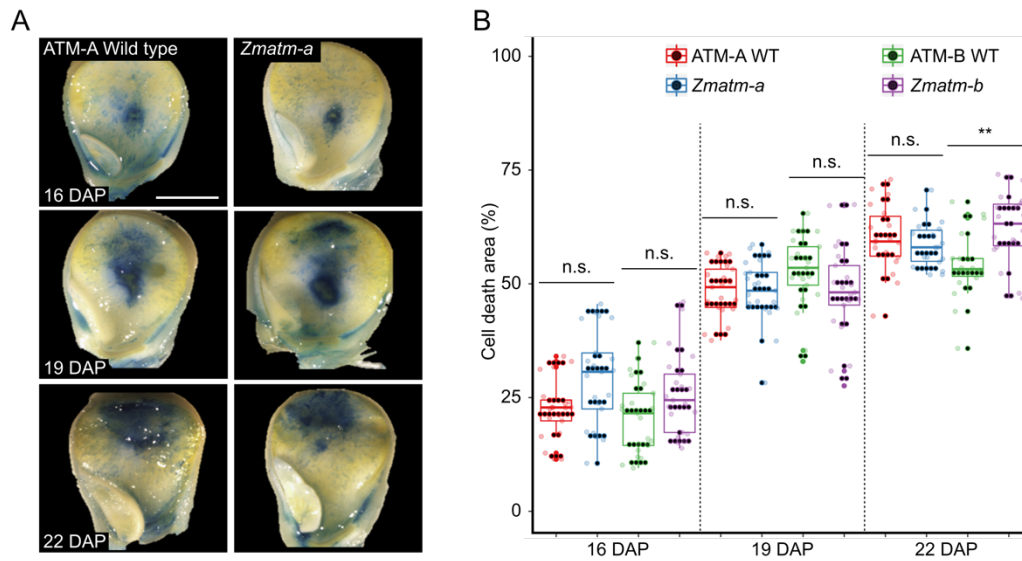
(B) Expression levels of replication initiation-related genes in *Zmatr-b* endosperm. RNA was extracted from an endosperm pool extracted from at least three kernels of three cobs for each genotype, and analyzed by RT-qPCR. The horizontal black line indicates the reference expression level of one unit in control samples (relative to wild-type sample of same genotype and time). Each bar shows the mean \pm SD of three biological replicates (*, $P < 0.001$, Student's *t*-test).



Supplemental Figure 10. Endoreduplication Is Not Affected in *Zmatm* Endosperm (Supports Figure 7).

(A) The mean C-value in wild-type (WT) ATM and mutant *Zmatm* endosperm at five developmental stages between 10 and 19 days after pollination (DAP).

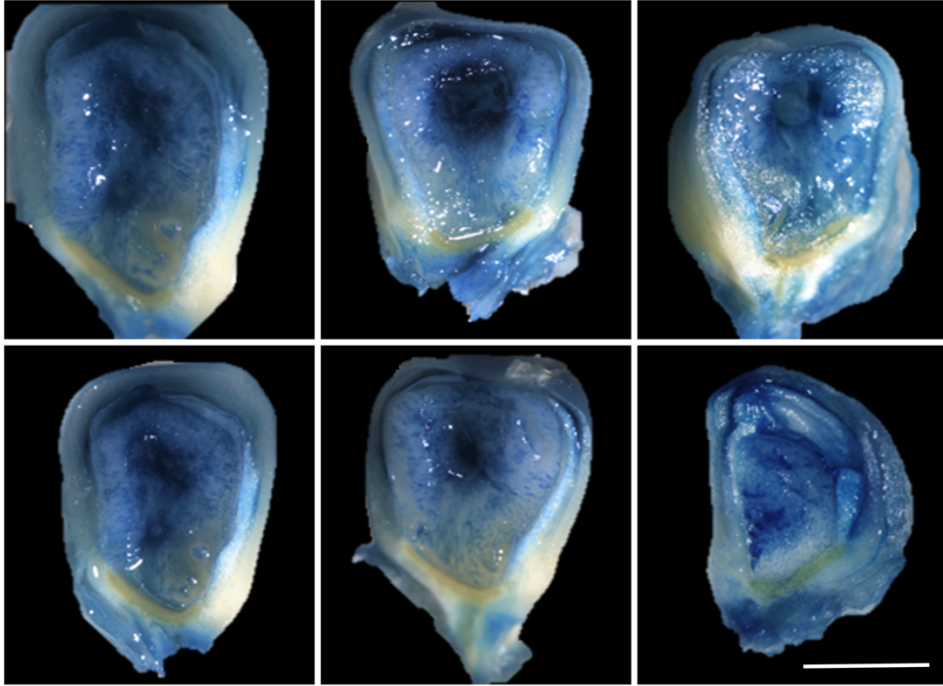
(B) Distribution of endosperm nuclei (expressed as a percentage of the total number of nuclei) among different ploidy classes in 19-DAP ATM-WT and *Zmatm* endosperms. Values are means ± SE; n=9-11, although no significant differences were found ($P < 0.001$, Student's *t*-test). All analyses were carried out from at least three kernels of three independent cobs for each genotype.



Supplemental Figure 11. *Zmatm* Endosperm Does Not Display Differences in Cell Death Timing or Abundance (Supports Figure 8).

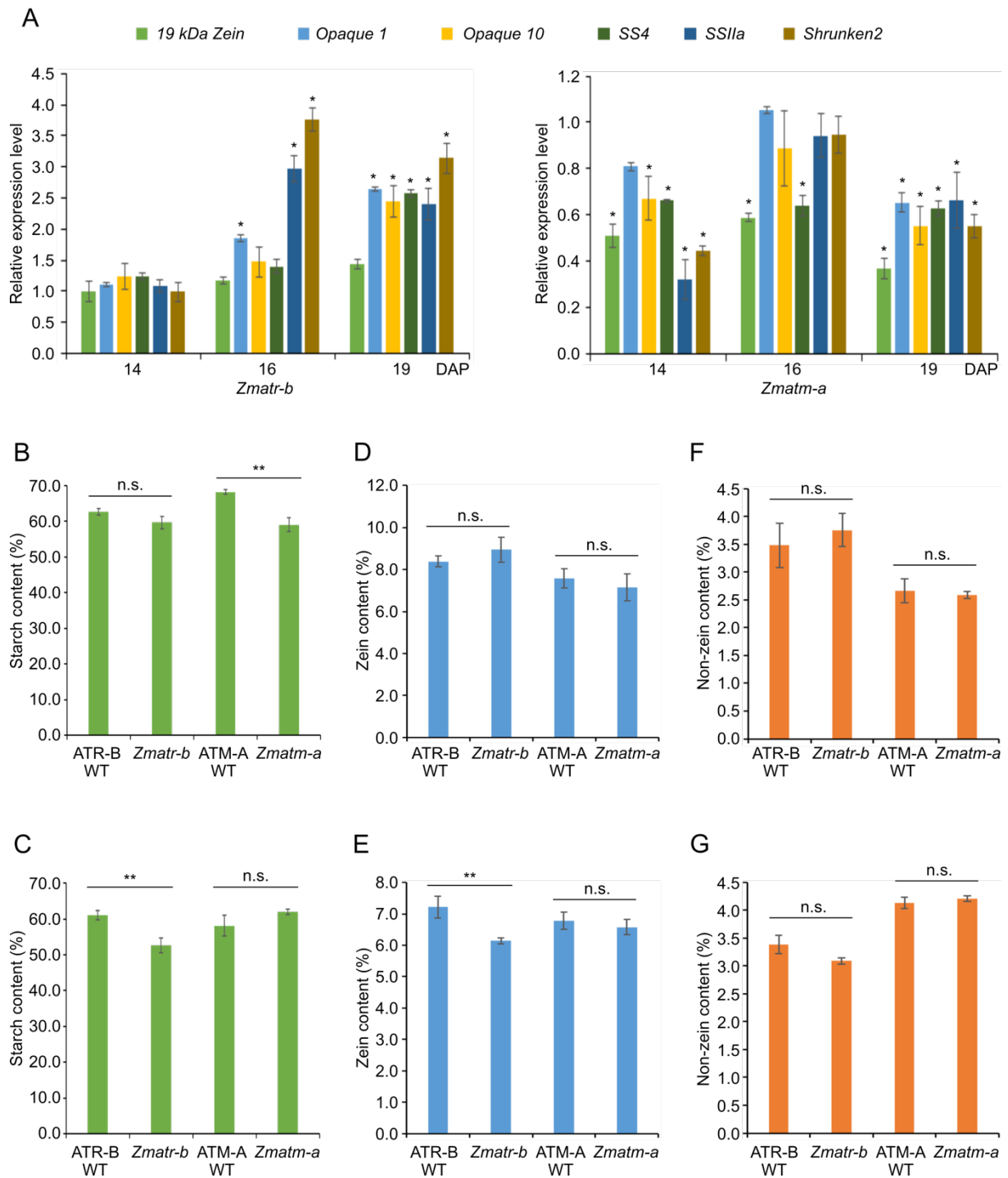
(A) Progression of endosperm cell death in ATM-A wild-type (WT) and *Zmatm-a* kernels as indicated by Evans Blue stain at indicated days after pollination (DAP). Scale bar = 3 mm.

(B) Quantification of the percentage of cell death within the endosperm area in ATM-A and ATM-B WT, and *Zmatm-a* and *Zmatm-b* mutants. All analyses were carried out from at least seven kernels of three independent cobs for each genotype. Values are means \pm SE; n=21 (**, $P < 0.005$, Student's *t*-test; n.s = no significant).



Supplemental Figure 12. Cell Death in Endosperm of *Zmatr* Aborted Kernels (Supports Figure 8).

Endosperm cell death in *Zmatr* abnormal kernels at 16 days after pollination, as indicated by Evans Blue stain. Scale bar = 3 mm.



Supplemental Figure 13. Starch and Protein Content in *Zmatr* and *Zmatm* Endosperm (Supports Figures 5, 7, and 8).

(A) Expression levels of genes associated with the zein and starch biosynthesis in endosperms of *Zmatr-b* and *Zmatm-a* at indicated days after pollination (DAP). RNA was extracted from an endosperm pool extracted from at least three kernels of three cobs for each genotype for RT-qPCR analysis. The horizontal black line indicates the reference expression level of one unit in control samples (respective

to wild-type sample of same genotype and time). Each bar shows the mean \pm SD (* $P < 0.05$, Student's *t*-test) of three biological replicates.

(B and C) Starch contents in *Zmatr* and *Zmatm* endosperm at 19 DAP (B) and in mature endosperm (C). Percentage represents mg per 100 mg of endosperm flour for each genotype. Values are means \pm SE; $n = 3$ (**, $P < 0.005$, Student's *t*-test; n.s = no significant).

(D-G) Zein (D, E) and non-zein (F, G) protein content (%) in *Zmatr* and *Zmatm* endosperm at 20 DAP (D and F) and in mature endosperm (E and G). Values are means \pm SE; $n = 3$ (**, $P < 0.005$, Student's *t*-test; n.s = not significant).

Supplemental Table 1. Percentage of Abnormal Kernels in *Zmatr* Cobs.

Line	Plant	Total kernels	# abnormal kernels	% abnormal kernels
<i>Zmatr-a</i>	1	254	15	5.9
	2	230	22	9.6
	3	185	12	6.5
	4	244	13	5.3
	5	210	36	17.1
<i>Zmatr-b</i>	1	165	14	8.5
	2	180	9	5.0
	3	194	12	6.2
	4	171	28	16.4
ATR-A WT	1	386	1	0.3
	2	335	0	0.0
	3	376	0	0.0
	4	281	2	0.7
	5	300	0	0.0
ATR-B WT	1	372	1	0.3
	2	352	2	0.6
	3	328	0	0.0
	4	270	0	0.0

Supplemental Table 2. Primers Used in This Study

CRISPR/Cas9 construct		qRT primers (sequence 5' to 3')	
Gene ID	Primer name	Forward	Reverse
	BAR-qRT	TGTCTCGATGTAGTGGTTGACG	ACACGCTGAAATCACCAGTC
	zCAS9-qRT	TAATGCTTGTGCTGCTCGAC	TGCCGTCCAAGTATGTGAAC

Genotyping of maize mutants		Primers (sequence 5' to 3')	
Gene ID	Gene name	Forward	Reverse
Zm00001d040166	ZmATM – target 1	GTAAGCTTCATGTGGAATGGGTC	AATGACCAGCAAAACAGGGAA
Zm00001d040166	ZmATM – target 2	ACATGTTCTATCCTCCAAGTACTGACT	ACACGAGATGGACTGGCCT
Zm00001d014813	ZmATR – target 1	CTGGAAGAGTGCAGAGGATATCC	GATTGCTCTGCACATCCTTTTAG
Zm00001d014813	ZmATR – target 2	CCTAAAGTTACTCTAGCAAGGGC	GGCGATCATGCCTTGAAGGT

qPCR for maize		qRT primers (sequence 5' to 3')	
Gene ID	Primer name	Forward	Reverse
Zm00001d036904	ZmEF-a-qRT	AGTCCGTTGAGATGCACCATG	CACATACCCACGCTTCAGATCC
AF16884.1	Zm18s rRNA-qRT	ACCTTACCAGCCCTTGACATATG	GACTTGACCAACATCTCAGCAC
Zm00001d014813	ZmATR-qRT	TCAAGCCTACAGGATCAGCT	ACTCCATGCATGCACCAAG
Zm00001d040166	ZmATM-qRT	GATGTACAGGAGTTTCATGCTTC	CGCAGATAGGTCACCTTCTACG
Zm00001d021898	ZmRAD51A-qRT	ACGCAGAGGGTACATTCAGACC	CAGCACCATTTCAGTCCAAACCTG
Zm00001d041757	ZmRAD51B-qRT	GTGCTAGCCAACCTTCATGCA	GAGTGTGGCACAACCTGAGTC
Zm00001d018151	ZmRAD54-qRT	TGTTCTGCTGGCGAAGAGGTTTC	TGAGCTGCTGATCGCACCATAG
Zm00001d038667	ZmBRCA1-qRT	CTCGCAAAAATAGCTGGTGTGC	AGAACTTCAGTGTGCGCTTGC
Zm00001d042357	ZmXRI1-qRT	GCAGACGCATGTTGCAGT	GTGAGCAATCGACTAGCCA
Zm00001d050104	ZmRAD7A-qRT	GAAATGCTGCACCAACACG	TGCTTGCATTGGCAGGATC
Zm00001d045192	ZmRNR1-qRT	ACTCATGCTTCACCGACG	GACACCAATTCTCCAGCAG
Zm00001d003164	ZmTSO2-qRT	AGAAGGCGTCCGTAATGTCCAG	AACTCAGAAGTCCCTCGTCCGATGC
Zm00001d027373	ZmCDKA1-qRT	CTTCGAGTACCTGGATCTGGA	CGCAACACCGTGGAGTATC
Zm00001d053998	ZmWEE1-qRT	GACTTCCTGAGCCACAATCTATG	GTCGTCGTCGAACTCGTTG
Zm00001d002662	ZmCyclinB2_1-qRT	AAGCTGCAGATGCAGATAAACAGC	GCTGGCAACGATTGATAGCACAC
Zm00001d015863	ZmBUBR1-qRT	TCAAAGTGTGGCTGGAATACGC	ACTCCAGCAACGATGCGTAAGAC

Zm00001d048497	ZmCDK2-qRT	CACGGCAACATCGTCAGGTTAC	TCTTAGCAAACCTCCGGGCAAGAG
Zm00001d032501	ZmBFN1-qRT	ACAGGAGATAACAACCTGACTGA	CGAGAGCCGTCTGTATGATCT
Zm00001d009594	ZmPASPA3-qRT	GCACTGGAATTCGTAGCGTA	GTAGGTCCAGGATGAGCTCCT
Zm00001d009392	ZmMCM3-qRT	GTGCCATGGTTCCTTGCTGATCGTGGTGT	GGAAAGCAGTGAATCCGGAAGCCCGATA
Zm00001d009374	ZmMCM4-qRT	GAGCTCGAGGTCTTGACTTGCAGACAC	TGCTTCGCTGAGACGGATCAAACCTCTCT
Zm00001d018384	ZmMCM5-qRT	AAAATGAGGCAGCAAGCTCACGAGACAG	ATCTTGCAGCATCAACGGTGGAGACATT
Zm00001d010406	ZmMCM6-qRT	ATGACCAAGCAGCGGATAATGG	ATGCCAGCTAAACCATCTCCATC
Zm00001d030614	ZmMCM7-qRT	GCAGAGCACGTACCAAAGGGCCACATTC	GCAACTAATCCTGCGCGCATCGCTCTAA
Zm00001d018415	ZmPCNA-qRT	CCATCGTCCGCATGCCTTCTTCTGAGTT	CAAAGGTCAGGGAAACCGGCTCTTGCAT
Zm00001d048851	Zm19kDa_zein-qRT	TTAGGTGGGACCCTATAGCCTTGC	ATGTGTCACACGTTTCCATTGGC
Zm00001d052110	ZmOpaque1-qRT	CAAAGTCAACACGTGGGCAAT	GCTGGGTGGGCACCAA
Zm00001d033654	ZmOpaque10-qRT	ATACCCTTGCTTGATGATG	GCTGAAGTCTGATGGCTC
Zm00001d010821	ZmSS4-qRT	ACCGGCGGTTTGAATGACAGTG	AGGTGAAGCCATTTTCGCACCTC
Zm00001d037234	ZmSSIIa-qRT	TGCTGTGCCACTCACTGTTTACC	TCAGCCCTAACGAGCAAAGGAC
Zm00001d044129	ZmShrunken2-qRT	TGGGAAGGTCCCAGTTGGAATAGG	TCAGCCTCTTGATGCCCTTAC

qPCR for *Arabidopsis thaliana*

qPCR for <i>Arabidopsis thaliana</i>		qRT primers (sequence 5' to 3')	
Gene ID	Primer name	Forward	Reverse
AT1G02780	EMB2386_qRT	CTCTCGTTCAGAGCTCGCAAAA	AAGAACACGCATCCTACGCATCC
AT3G22110	PAC1_qRT	TCTCTTTGCAGGATGGGACAAGC	AGACTGAGCCGCCTGATTGTTTG
AT3G56340	RPS26E_qRT	GACTTTCAAGCGCAGGAATGGTG	CCTTGTCCCTGGGGCAACACTTT
AT5G20850	RAD51A-qRT	GACTCTTACAGATAGCTGACAGGT	GCGGTAGCACTATCGACAATC
AT2G28560	RAD51B-qRT	GAGCTCAGAGACAACCTCAGT	ATACTGACTAGTTTCATCGCGGT
AT4G21070	BRCA1-qRT	AGGTGAACCTGTCTCTGCGGATTT	TTCTCCGGCTTCTTGTCAACTCCA
AT5G48720	XRI1-qRT	GCTACCTGATGACTTAAACTTTGGTTC	CATTTGGAGAAGATCGAGTCACAG
AT2G06040	RAD7A-qRT	CGATTCTTCGATCTCGCGAAAT	GTAGTGTGAGTGGGTTTCATCAAC
AT4G37490	CYCB1-1-qRT	GGAAGCAACAAGAAGAAGGGAG	AGGGATCAAAGCCACAGCG
AT2G31320	PARP2-qRT	AGCCTGAAGGCCCGGTAACA	GCTGTCTCAGTTTTGGCTGCCG
AT5G02220	SMR4-qRT	GAAGGATGTACGACGCCGA	TCTTCGAGGCTGTGCGTAG
AT1G07500	SMR5-qRT	AAACTACGACGACGGAGATACG	GCTACCACCGAGAAGAACAAGT
AT3G27630	SMR7-qRT	GCCAAAACATCGATTCGGGCTTC	TCGCCGTGGGAGTGATACAAAT

Parsed Citations

Adachi, S., Minamisawa, K., Okushima, Y., Inagaki, S., Yoshiyama, K., Kondou, Y., Kaminuma, E., Kawashima, M., Toyoda, T., Matsui, M., Kurihara, D., Matsunaga, S., and Umeda, M. (2011). Programmed induction of endoreduplication by DNA double-strand breaks in *Arabidopsis*. *Proc. Natl. Acad. Sci. USA* 108, 10004-10009.

Google Scholar: [Author Only](#) [Title Only](#) [Author and Title](#)

Amiard, S., Charbonnel, C., Allain, E., Depeiges, A., White, C.I., and Gallego, M.E. (2010). Distinct roles of the ATR kinase and the Mre11-Rad50-Nbs1 complex in the maintenance of chromosomal stability in *Arabidopsis*. *Plant Cell* 22, 3020-3033.

Google Scholar: [Author Only](#) [Title Only](#) [Author and Title](#)

Biedermann, S., Harashima, H., Chen, P., Heese, M., Bouyer, D., Sofroni, K., and Schnittger, A. (2017). The retinoblastoma homolog RBR1 mediates localization of the repair protein RAD51 to DNA lesions in *Arabidopsis*. *EMBO J.* 36, 1279-1297.

Google Scholar: [Author Only](#) [Title Only](#) [Author and Title](#)

Blackford, A.N., and Jackson, S.P. (2017). ATM, ATR, and DNA-PK: the trinity at the heart of the DNA damage response. *Mol. Cell* 66, 801-817.

Google Scholar: [Author Only](#) [Title Only](#) [Author and Title](#)

Bourbousse, C., Vegesna, N., and Law, J.A. (2018). SOG1 activator and MYB3R repressors regulate a complex DNA damage network in *Arabidopsis*. *Proc. Natl. Acad. Sci. USA* 115, E12453-E12462.

Google Scholar: [Author Only](#) [Title Only](#) [Author and Title](#)

Brown, E.J., and Baltimore, D. (2000). ATR disruption leads to chromosomal fragmentation and early embryonic lethality. *Genes Dev.* 14, 397-402.

Google Scholar: [Author Only](#) [Title Only](#) [Author and Title](#)

Cimprich, K.A., and Cortez, D. (2008). ATR: an essential regulator of genome integrity. *Nat. Rev. Mol. Cell Biol.* 9, 616-627.

Google Scholar: [Author Only](#) [Title Only](#) [Author and Title](#)

Cools, T., Iantcheva, A., Weimer, A.K., Boens, S., Takahashi, N., Maes, S., Van den Daele, H., Van Isterdael, G., Schnittger, A., and De Veylder, L. (2011). The *Arabidopsis thaliana* checkpoint kinase WEE1 protects against premature vascular differentiation during replication stress. *Plant Cell* 23, 1435-1448.

Google Scholar: [Author Only](#) [Title Only](#) [Author and Title](#)

Coussens, G., Aesaert, S., Verelst, W., Demeulenaere, M., De Buck, S., Njuguna, E., Inzé, D., and Van Lijsebettens, M. (2012). *Brachypodium distachyon* promoters as efficient building blocks for transgenic research in maize. *J. Exp. Bot.* 63, 4263-4273.

Google Scholar: [Author Only](#) [Title Only](#) [Author and Title](#)

Craven, R.J., Greenwell, P.W., Dominska, M., and Petes, T.D. (2002). Regulation of genome stability by TEL1 and MEC1, yeast homologs of the mammalian ATM and ATR genes. *Genetics* 161, 493-507.

Google Scholar: [Author Only](#) [Title Only](#) [Author and Title](#)

Culligan, K., Tissier, A., and Britt, A. (2004). ATR regulates a G2-phase cell-cycle checkpoint in *Arabidopsis thaliana*. *Plant Cell* 16, 1091-1104.

Google Scholar: [Author Only](#) [Title Only](#) [Author and Title](#)

Culligan, K.M., and Britt, A.B. (2008). Both ATM and ATR promote the efficient and accurate processing of programmed meiotic double-strand breaks. *Plant J.* 55, 629-638.

Google Scholar: [Author Only](#) [Title Only](#) [Author and Title](#)

Culligan, K.M., Robertson, C.E., Foreman, J., Doerner, P., and Britt, A.B. (2006). ATR and ATM play both distinct and additive roles in response to ionizing radiation. *Plant J.* 48, 947-961.

Google Scholar: [Author Only](#) [Title Only](#) [Author and Title](#)

Doll, N.M., Depège-Fargeix, N., Rogowsky, P.M., and Widiez, T. (2017). Signaling in early maize kernel development. *Mol. Plant* 10, 375-388.

Google Scholar: [Author Only](#) [Title Only](#) [Author and Title](#)

Dominguez, F., and Cejudo, F.J. (2014). Programmed cell death (PCD): an essential process of cereal seed development and germination. *Front. Plant Sci.* 5, 366.

Google Scholar: [Author Only](#) [Title Only](#) [Author and Title](#)

Farage-Barhom, S., Burd, S., Sonogo, L., Perl-Treves, R., and Lers, A. (2008). Expression analysis of the BFN1 nuclease gene promoter during senescence, abscission, and programmed cell death-related processes. *J. Exp. Bot.* 59, 3247-3258.

Google Scholar: [Author Only](#) [Title Only](#) [Author and Title](#)

Fendrych, M., Van Hautegeem, T., Van Durme, M., Olivera-Carrillo, Y., Huysmans, M., Karimi, M., Lippens, S., Guérin, C.J., Krebs, M., Schumacher, K., and Nowack, M.K. (2014). Programmed cell death controlled by ANAC033/SOMBRERO determines root cap organ size in *Arabidopsis*. *Curr. Biol.* 24, 931-940.

Google Scholar: [Author Only](#) [Title Only](#) [Author and Title](#)

Friedel, A.M., Pike, B.L., and Gasser, S.M. (2009). ATR/Mec1: coordinating fork stability and repair. *Curr. Opin. Cell Biol.* 21, 237-244.

Google Scholar: [Author Only](#) [Title Only](#) [Author and Title](#)

Friesner, J.D., Liu, B., Culligan, K., and Britt, A.B. (2005). Ionizing radiation-dependent γ -H2AX focus formation requires ataxia telangiectasia mutated and ataxia telangiectasia mutated and Rad3-related. *Mol. Biol. Cell* 16, 2566-2576.

Google Scholar: [Author Only](#) [Title Only](#) [Author and Title](#)

Fulcher, N., and Sablowski, R. (2009). Hypersensitivity to DNA damage in plant stem cell niches. *Proc. Natl. Acad. Sci. USA* 106, 20984-20988.

Google Scholar: [Author Only](#) [Title Only](#) [Author and Title](#)

Furukawa, T., Curtis, M.J., Tominey, C.M., Duong, Y.H., Wilcox, B.W.L., Aggoune, D., Hays, J.B., and Britt, A.B. (2010). A shared DNA-damage-response pathway for induction of stem-cell death by UVB and by gamma irradiation. *DNA Repair* 9, 940-948.

Google Scholar: [Author Only](#) [Title Only](#) [Author and Title](#)

Garcia, V., Bruchet, H., Camescasse, D., Granier, F., Bouchez, D., and Tissier, A. (2003). AtATM is essential for meiosis and the somatic response to DNA damage in plants. *Plant Cell* 15, 119-132.

Google Scholar: [Author Only](#) [Title Only](#) [Author and Title](#)

Gasch, A.P., Huang, M., Metzner, S., Botstein, D., Elledge, S.J., and Brown, P.O. (2001). Genomic expression responses to DNA-damaging agents and the regulatory role of the yeast ATR homolog Mec1p. *Mol. Biol. Cell* 12, 2987-3003.

Google Scholar: [Author Only](#) [Title Only](#) [Author and Title](#)

Gu, N., Tamada, Y., Imai, A., Palfalvi, G., Kabeya, Y., Shigenobu, S., Ishikawa, M., Angelis, K.J., Chen, C., and Hasebe, M. (2020). DNA damage triggers reprogramming of differentiated cells into stem cells in *Physcomitrella*. *Nat. Plants* 6, 1098-1105.

Google Scholar: [Author Only](#) [Title Only](#) [Author and Title](#)

Haberer, G., Young, S., Bharti, A.K., Gundlach, H., Raymond, C., Fuks, G., Butler, E., Wing, R.A., Rounsley, S., Birren, B., Nusbaum, C., Mayer, K.F.X., and Messing, J. (2005). Structure and architecture of the maize genome. *Plant Physiol.* 139, 1612-1624.

Google Scholar: [Author Only](#) [Title Only](#) [Author and Title](#)

He, Y., Wang, J., Qi, W., and Song, R. (2019). Maize Dek15 encodes the cohesin-loading complex subunit SCC4 and is essential for chromosome segregation and kernel development. *Plant Cell* 31, 465-485.

Google Scholar: [Author Only](#) [Title Only](#) [Author and Title](#)

Hu, Z., Cools, T., and De Veylder, L. (2016). Mechanisms used by plants to cope with DNA damage. *Annu. Rev. Plant Biol.* 67, 439-462.

Google Scholar: [Author Only](#) [Title Only](#) [Author and Title](#)

Iyer, D.R., and Rhind, N. (2017). The intra-S checkpoint responses to DNA damage. *Genes* 8, 74.

Google Scholar: [Author Only](#) [Title Only](#) [Author and Title](#)

Jaehnig, E.J., Kuo, D., Hombauer, H., Ideker, T.G., and Kolodner, R.D. (2013). Checkpoint kinases regulate a global network of transcription factors in response to DNA damage. *Cell Reports* 4, 174-188.

Google Scholar: [Author Only](#) [Title Only](#) [Author and Title](#)

Jossen, R., and Bermejo, R. (2013). The DNA damage checkpoint response to replication stress: A Game of Forks. *Front. Genet.* 4, 26.

Google Scholar: [Author Only](#) [Title Only](#) [Author and Title](#)

Kim, J.-H., Ryu, T.H., Lee, S.S., Lee, S., and Chung, B.Y. (2019). Ionizing radiation manifesting DNA damage response in plants: an overview of DNA damage signaling and repair mechanisms in plants. *Plant Sci.* 278, 44-53.

Google Scholar: [Author Only](#) [Title Only](#) [Author and Title](#)

Lahari, T., Lazaro, J., Marcus, J.M., and Schroeder, D.F. (2018). RAD7 homologues contribute to Arabidopsis UV tolerance. *Plant Sci.* 277, 267-277.

Google Scholar: [Author Only](#) [Title Only](#) [Author and Title](#)

Lei, Y., Lu, L., Liu, H.-Y., Li, S., Xing, F., and Chen, L.-L. (2014). CRISPR-P: a web tool for synthetic single-guide RNA design of CRISPR-system in plants. *Mol. Plant* 7, 1494-1496.

Google Scholar: [Author Only](#) [Title Only](#) [Author and Title](#)

Li, Z., Kim, J.H., Kim, J., Lyu, J.I., Zhang, Y., Guo, H., Nam, H.G., and Woo, H.R. (2020). ATM suppresses leaf senescence triggered by DNA double-strand break through epigenetic control of senescence-associated genes in *Arabidopsis*. *New Phytol.* 227, 473-484.

Google Scholar: [Author Only](#) [Title Only](#) [Author and Title](#)

Manova, V., and Gruszka, D. (2015). DNA damage and repair in plants – from models to crops. *Front. Plant Sci.* 6, 885.

Google Scholar: [Author Only](#) [Title Only](#) [Author and Title](#)

Mantiero, D., Clerici, M., Lucchini, G., and Longhese, M.P. (2007). Dual role for *Saccharomyces cerevisiae* Tel1 in the checkpoint response to double-strand breaks. *EMBO Rep.* 8, 380-387.

Google Scholar: [Author Only](#) [Title Only](#) [Author and Title](#)

Maréchal, A., and Zou, L. (2013). DNA damage sensing by the ATM and ATR kinases. *Cold Spring Harb. Perspect. Biol.* 5, a012716.

Google Scholar: [Author Only](#) [Title Only](#) [Author and Title](#)

Martens, M., Horres, R., Wendeler, E., and Reiss, B. (2020). The importance of ATM and ATR in *Physcomitrella patens* DNA damage

repair, development, and gene targeting. *Genes* 11, 752.

Google Scholar: [Author Only Title Only Author and Title](#)

Menolfi, D., and Zha, S. (2020). ATM, ATR and DNA-PKcs kinases - the lessons from the mouse models: inhibition ≠ deletion. *Cell Biosci.* 10, 8.

Google Scholar: [Author Only Title Only Author and Title](#)

Moussu, S., Doll, N.M., Chamot, S., Brocard, L., Creff, A., Fourquin, C., Widiez, T., Nimchuk, Z.L., and Ingram, G. (2017). ZHOUP1 and KERBEROS mediate embryo/endosperm separation by promoting the formation of an extracuticular sheath at the embryo surface. *Plant Cell* 29, 1642-1656.

Google Scholar: [Author Only Title Only Author and Title](#)

Murga, M., Bunting, S., Montaña, M.F., Soria, R., Mulero, F., Cañamero, M., Lee, Y., McKinnon, P.J., Nussenzweig, A., and Fernandez-Capetillo, O. (2009). A mouse model of ATR-Seckel shows embryonic replicative stress and accelerated aging. *Nat. Genet.* 41, 891-898.

Google Scholar: [Author Only Title Only Author and Title](#)

Nikitaki, Z., Holá, M., Donà, M., Pavlopoulou, A., Michalopoulos, I., Angelis, K.J., Georgakilas, A.G., Macovei, A., and Balestrazzi, A. (2018). Integrating plant and animal biology for the search of novel DNA damage biomarkers. *Mutat. Res.* 775, 21-38.

Google Scholar: [Author Only Title Only Author and Title](#)

Nisa, M.U., Huang, Y., Benhamed, M., and Raynaud, C. (2019). The plant DNA damage response: signaling pathways leading to growth inhibition and putative role in response to stress conditions. *Front. Plant Sci.* 10, 653.

Google Scholar: [Author Only Title Only Author and Title](#)

Ogita, N., Okushima, Y., Tokizawa, M., Yamamoto, Y.Y., Tanaka, M., Seki, M., Makita, Y., Matsui, M., Okamoto-Yoshiyama, K., Sakamoto, T., Kurata, T., Hiruma, K., Saijo, Y., Takahashi, N., and Umeda, M. (2018). Identifying the target genes of SUPPRESSOR OF GAMMA RESPONSE 1, a master transcription factor controlling DNA damage response in *Arabidopsis*. *Plant J.* 94, 439-453.

Google Scholar: [Author Only Title Only Author and Title](#)

Peterson, R., Slovin, J.P., and Chen, C. (2010). A simplified method for differential staining of aborted and non-aborted pollen grains. *Int. J. Plant Biol.* 1, e13.

Google Scholar: [Author Only Title Only Author and Title](#)

Ricaud, L., Proux, C., Renou, J.-P., Pichon, O., Fochesato, S., Ortet, P., and Montané, M.-H. (2007). ATM-mediated transcriptional and developmental responses to γ -rays in *Arabidopsis*. *PLoS ONE* 2, e430.

Google Scholar: [Author Only Title Only Author and Title](#)

Roa, H., Lang, J., Culligan, K.M., Keller, M., Holec, S., Cognat, V., Montané, M.-H., Houlné, G., and Chabouté, M.-E. (2009). Ribonucleotide reductase regulation in response to genotoxic stress in *Arabidopsis*. *Plant Physiol.* 151, 461-471.

Google Scholar: [Author Only Title Only Author and Title](#)

Roitinger, E., Hofer, M., Köcher, T., Pichler, P., Novatchkova, M., Yang, J., Schlögelhofer, P., and Mechtler, K. (2015). Quantitative phosphoproteomics of the ataxia telangiectasia-mutated (ATM) and ataxia telangiectasia-mutated and rad3-related (ATR) dependent DNA damage response in *Arabidopsis thaliana*. *Mol. Cell. Proteomics* 14, 556-571.

Google Scholar: [Author Only Title Only Author and Title](#)

Sabelli, P.A., and Larkins, B.A. (2009). The contribution of cell cycle regulation to endosperm development. *Sex. Plant Reprod.* 22, 207-219.

Google Scholar: [Author Only Title Only Author and Title](#)

Sánchez-Pons, N., Irar, S., García-Muniz, N., and Vicent, C.M. (2011). Transcriptomic and proteomic profiling of maize embryos exposed to camptothecin. *BMC Plant Biol.* 11, 91.

Google Scholar: [Author Only Title Only Author and Title](#)

Schnable, P.S., Ware, D., Fulton, R.S., Stein, J.C., Wei, F., Pasternak, S., Liang, C., Zhang, J., Fulton, L., Graves, T.A., Minx, P., Reily, A.D., Courtney, L., Kruchowski, S.S., Tomlinson, C., Strong, C., Delehaunty, K., Fronick, C., Courtney, B., Rock, S.M., Belter, E., Du, F., Kim, K., Abbott, R.M., Cotton, M., Levy, A., Marchetto, P., Ochoa, K., Jackson, S.M., Gillam, B., Chen, W., Yan, L., Higginbotham, J., Cardenas, M., Waligorski, J., Applebaum, E., Phelps, L., Falcone, J., Kanchi, K., Thane, T., Scimone, A., Thane, N., Henke, J., Wang, T., Ruppert, J., Shah, N., Rotter, K., Hodges, J., Ingenthron, E., Cordes, M., Kohlberg, S., Sgro, J., Delgado, B., Mead, K., Chinwalla, A., Leonard, S., Crouse, K., Collura, K., Kudrna, D., Currie, J., He, R., Angelova, A., Rajasekar, S., Mueller, T., Lomeli, R., Scara, G., Ko, A., Delaney, K., Wissotski, M., Lopez, G., Campos, D., Braidotti, M., Ashley, E., Golser, W., Kim, Y., Lee, S., Lin, J., Dujmic, Z., Kim, W., Talag, J., Zuccolo, A., Fan, C., Sebastian, A., Kramer, M., Spiegel, L., Nascimento, L., Zutavern, T., Miller, B., Ambroise, C., Muller, S., Spooner, W., Narechania, A., Ren, L., Wei, S., Kumari, S., Faga, B., Levy, M.J., McMahan, L., Van Buren, P., Vaughn, M.W., Ying, K., Yeh, C.-T., Enrich, S.J., Jia, Y., Kalyanaraman, A., Hsia, A.-P., Barbazuk, W.B., Baucom, R.S., Brutnell, T.P., Carpita, N.C., Chaparro, C., Chia, J.-M., Deragon, J.-M., Estill, J.C., Fu, Y., Jeddalo, J.A., Han, Y., Lee, H., Li, P., Lisch, D.R., Liu, S., Liu, Z., Nagel, D.H., McCann, M.C., SanMiguel, P., Myers, A.M., Nettleton, D., Nguyen, J., Penning, B.W., Ponnala, L., Schneider, K.L., Schwartz, D.C., Sharma, A., Soderlund, C., Springer, N.M., Sun, Q., Wang, H., Waterman, M., Westerman, R., Wolfgruber, T.K., Yang, L., Yu, Y., Zhang, L., Zhou, S., Zhu, Q., Bennetzen, J.L., Dawe, R.K., Jiang, J., Jiang, N., Presting, G.G., Wessler, S.R., Aluru, S., Martienssen, R.A., Clifton, S.W., McCombie, W.R., Wing, R.A., and Wilson, R.K. (2009). The B73 maize genome: complexity, diversity, and dynamics. *Science* 326, 1112-1115.

Google Scholar: [Author Only Title Only Author and Title](#)

Segurado, M., and Tercero, J.A. (2009). The S-phase checkpoint: targeting the replication fork. *Biol. Cell* 101, 617-627.

Google Scholar: [Author Only](#) [Title Only](#) [Author and Title](#)

Singh, A., and Xu, Y.-J. (2016). The cell killing mechanisms of hydroxyurea. *Genes* 7, 99.

Google Scholar: [Author Only](#) [Title Only](#) [Author and Title](#)

Sjogren, C.A., Bolaris, S.C., and Larsen, P.B. (2015). Aluminum-dependent terminal differentiation of the Arabidopsis root tip is mediated through an ATR-, ALT2-, and SOG1-regulated transcriptional response. *Plant Cell* 27, 2501-2515.

Google Scholar: [Author Only](#) [Title Only](#) [Author and Title](#)

Stelpflug, S.C., Sekhon, R.S., Vaillancourt, B., Hirsch, C.N., Buell, C.R., de Leon, N., and Kaeppeler, S.M. (2016). An expanded maize gene expression atlas based on RNA sequencing and its use to explore root development. *Plant Genome* 9, 1-16.

Google Scholar: [Author Only](#) [Title Only](#) [Author and Title](#)

Szurman-Zubrzycka, M.E., Nawrot, M., Jelonek, J., Dziekanowski, M., Kwasniewska, J., and Szarejko, I. (2019). ATR, a DNA damage signaling kinase, is involved in aluminum response in barley. *Front. Plant Sci.* 10, 1299.

Google Scholar: [Author Only](#) [Title Only](#) [Author and Title](#)

Tomimatsu, N., Mukherjee, B., and Burma, S. (2009). Distinct roles of ATR and DNA-PKcs in triggering DNA damage responses in ATM-deficient cells. *EMBO Rep.* 10, 629-635.

Google Scholar: [Author Only](#) [Title Only](#) [Author and Title](#)

Turinetto, V., and Giachino, C. (2015). Multiple facets of histone variant H2AX: a DNA double-strand-break marker with several biological functions. *Nucleic Acids Res.* 43, 2489-2498.

Google Scholar: [Author Only](#) [Title Only](#) [Author and Title](#)

Van Bel, M., Diels, T., Vancaester, E., Kreft, L., Botzki, A., Van de Peer, Y., Coppens, F., and Vandepoele, K. (2018). PLAZA 4.0: an integrative resource for functional, evolutionary and comparative plant genomics. *Nucleic Acids Res.* 46, D1190-D1196.

Google Scholar: [Author Only](#) [Title Only](#) [Author and Title](#)

Wang, H., Wang, H., Powell, S.N., Iliakis, G., and Wang, Y. (2004). ATR affecting cell radiosensitivity is dependent on homologous recombination repair but independent of nonhomologous end joining. *Cancer Res.* 64, 7139-7143.

Google Scholar: [Author Only](#) [Title Only](#) [Author and Title](#)

Waterworth, W.M., Bray, C.M., and West, C.E. (2015). The importance of safeguarding genome integrity in germination and seed longevity. *J. Exp. Bot.* 66, 3549-3558.

Google Scholar: [Author Only](#) [Title Only](#) [Author and Title](#)

Waterworth, W.M., Footitt, S., Bray, C.M., Finch-Savage, W.E., and West, C.E. (2016). DNA damage checkpoint kinase ATM regulates germination and maintains genome stability in seeds. *Proc. Natl. Acad. Sci. USA* 113, 9647-9652.

Google Scholar: [Author Only](#) [Title Only](#) [Author and Title](#)

Waterworth, W.M., Wilson, M., Wang, D., Nuhse, T., Warward, S., Selley, J., and West, C.E. (2019). Phosphoproteomic analysis reveals plant DNA damage signalling pathways with a functional role for histone H2 AX phosphorylation in plant growth under genotoxic stress. *Plant J.* 100, 1007-1021.

Google Scholar: [Author Only](#) [Title Only](#) [Author and Title](#)

Watson, A., Mata, J., Bähler, J., Carr, A., and Humphrey, T. (2004). Global gene expression responses of fission yeast to ionizing radiation. *Mol. Biol. Cell* 15, 851-860.

Google Scholar: [Author Only](#) [Title Only](#) [Author and Title](#)

Xing, H.-L., Dong, L., Wang, Z.-P., Zhang, H.-Y., Han, C.-Y., Liu, B., Wang, X.-C., and Chen, Q.-J. (2014). A CRISPR/Cas9 toolkit for multiplex genome editing in plants. *BMC Plant Biol.* 14, 327.

Google Scholar: [Author Only](#) [Title Only](#) [Author and Title](#)

Yi, D., Lessa Alvim Kamei, C., Cools, T., Vanderauwera, S., Takahashi, N., Okushima, Y., Eekhout, T., Yoshiyama, K.O., Larkin, J., Van den Daele, H., Conklin, P., Britt, A., Umeda, M., and De Veylder, L. (2014). The Arabidopsis SIAMESE-RELATED cyclin-dependent kinase inhibitors SMR5 and SMR7 regulate the DNA damage checkpoint in response to reactive oxygen species. *Plant Cell* 26, 296-309.

Google Scholar: [Author Only](#) [Title Only](#) [Author and Title](#)

Yoshiyama, K., Conklin, P.A., Huefner, N.D., and Britt, A.B. (2009). Suppressor of gamma response 1 (SOG1) encodes a putative transcription factor governing multiple responses to DNA damage. *Proc. Natl. Acad. Sci. USA* 106, 12843-12848.

Google Scholar: [Author Only](#) [Title Only](#) [Author and Title](#)

Yoshiyama, K.O., Sakaguchi, K., and Kimura, S. (2013a). DNA damage response in plants: conserved and variable response compared to animals. *Biology* 2, 1338-1356.

Google Scholar: [Author Only](#) [Title Only](#) [Author and Title](#)

Yoshiyama, K.O., Kaminoyama, K., Sakamoto, T., and Kimura, S. (2017). Increased phosphorylation of Ser-Gln sites on SUPPRESSOR OF GAMMA RESPONSE1 strengthens the DNA damage response in Arabidopsis thaliana. *Plant Cell* 29, 3255-3268.

Google Scholar: [Author Only](#) [Title Only](#) [Author and Title](#)

Yoshiyama, K.O., Kobayashi, J., Ogita, N., Ueda, M., Kimura, S., Maki, H., and Umeda, M. (2013b). ATM-mediated phosphorylation of SOG1 is essential for the DNA damage response in Arabidopsis. *EMBO Rep.* 14, 817-822.

Google Scholar: [Author Only](#) [Title Only](#) [Author and Title](#)

Young, T.E., and Gallie, D.R. (2000). Regulation of programmed cell death in maize endosperm by abscisic acid. *Plant Mol. Biol. Rep.* 42, 397-414.

Google Scholar: [Author Only](#) [Title Only](#) [Author and Title](#)

Young, T.E., Gallie, D.R., and DeMason, D.A (1997). Ethylene-mediated programmed cell death during maize endosperm development of wild-type and *shrunken2* genotypes. *Plant Physiol.* 115, 737-751.

Google Scholar: [Author Only](#) [Title Only](#) [Author and Title](#)

Zhang, C., Zhang, F., Cheng, X., Liu, K., Tang, J., Li, Y., Tang, D., Cheng, Z., and Yu, H. (2020). OsATM safeguards accurate repair of meiotic double-strand breaks in rice. *Plant Physiol.* 183, 1047-1057.

Google Scholar: [Author Only](#) [Title Only](#) [Author and Title](#)

Zhang, Z., Dong, J., Ji, C., Wu, Y., and Messing, J. (2019). NAC-type transcription factors regulate accumulation of starch and protein in maize seeds. *Proc. Natl. Acad. Sci. USA* 116, 11223-11228.

Google Scholar: [Author Only](#) [Title Only](#) [Author and Title](#)